Quaternary Science Reviews 231 (2020) 106173

Contents lists available at ScienceDirect

Quaternary Science Reviews

journal homepage: www.elsevier.com/locate/quascirev

Holocene changes in sea-ice cover and polynya formation along the eastern North Greenland shelf: New insights from biomarker records

Nicole Syring [a, *], Ruediger Stein [a, b], Kirsten Fahl [a], Maximilian Vahlenkamp [b], Marc Zehnich [c, d], Robert F. Spielhagen [d], Frank Niessen [a]

[a] Alfred Wegener Institute Helmholtz Centre for Polar and Marine Research (AWI), Am Alten Hafen 26, Bremerhaven, 27568, Germany
[b] Faculty of Geosciences (FB5), University of Bremen, Klagenfurter Str. 4, Bremen, 28359, Germany
[c] Academy of Sciences, Humanities and Literature, Geschwister-Scholl-Str. 2, 55131, Mainz, Germany
[d] GEOMAR Helmholtz Centre for Ocean Research, Wischhofstr. 1-3, Geb. 4, 24148, Kiel, Germany

ARTICLE INFO

Article history:
Received 15 May 2019
Received in revised form
16 January 2020
Accepted 16 January 2020
Available online 30 January 2020

ABSTRACT

Understanding the processes controlling the natural variability of sea ice in the Arctic, one of the most dynamic components of the climate system, can help to constrain the effects of future climate change in this highly sensitive area. For the first time, a high-resolution biomarker study was carried out to reconstruct past sea-ice variability off eastern North Greenland. This area is strongly influenced by cold surface waters and drift ice transported via the East Greenland Current, meltwater pulses from the outlet glaciers of the Northeast Greenland Ice Stream and the build-up of landfast ice. The well-dated Holocene sedimentary section of Core PS93/025 provides insights into variations of the sea-ice conditions (regional and local sea-ice signal), oceanic and atmospheric circulation and the biotic response to these changes. These biomarker records show a reduced to variable sea-ice cover during the early Holocene between 10.2 and 9.3 ka, followed by a steady increase in sea-ice conditions during the mid Holocene. During the last 5–6 ka, sea-ice conditions remained more stable representing a seasonal to marginal sea-ice situation. Based on our biomarker records, stable sea-ice edge conditions, with a fully developed polynya situation occurred since the last 1 ka.

1. Introduction

1.1. Background

Arctic sea ice is a key component in our climate system, regulating the global heat budget, influencing the atmospheric circulation (Serreze et al., 2016) and the global ocean circulation via the Atlantic Meridional Overturning Circulation (AMOC; Sévellec et al., 2017). Alternations in Arctic sea-ice extent can result in major changes to deep-water formation in the Nordic Seas (Rudels and Quadfasel, 1991) and lower latitudinal climate of the North Atlantic region (Overland and Wang, 2005). Thus, the recent dramatic loss of Arctic sea ice (Fig. 1) can affect global climate beyond the polar regions, changing the planetary albedo, surface heat and freshwater flux (Thomas and Dieckmann, 2008; Sévellec et al., 2017). Sea ice is not only an important factor for biodiversity and -productivity in the Arctic, providing a habitat to ice-associated species including organisms such as sea ice-algae, fish, birds, and marine mammals (Rudels et al., 1996; Dieckmann and Hellmer, 2003), it also acts as insulating layer between the ocean and the atmosphere (Stroeve et al., 2012).

The particular importance of Arctic sea ice with respect to recent anthropogenic climate change is that it is one of the most dynamic components of the climate system. Due to a reduction in the ice-ocean albedo effect, declining Arctic sea ice is expected to amplify anthropogenic climate change in the polar regions (Manabe et al., 1992; Randall et al., 1998; Screen and Simmonds, 2010). Over the past three decades, summer sea-ice extent and thickness have declined by 50%, much faster than predicted by climate models (see review by Stroeve et al., 2012; Serreze et al., 2016; Walsh et al., 2017; Notz and Stroeve, 2018).

The oceanographic and sea-ice conditions on the eastern North Greenland shelf are influenced by the outflow of freshwater and sea ice (drift ice) from the central Arctic Ocean, as well as by rivers, fjords, islands and marine-terminating outlet glaciers from the

* Corresponding author.
E-mail address: nsyring@awi.de (N. Syring).

https://doi.org/10.1016/j.quascirev.2020.106173

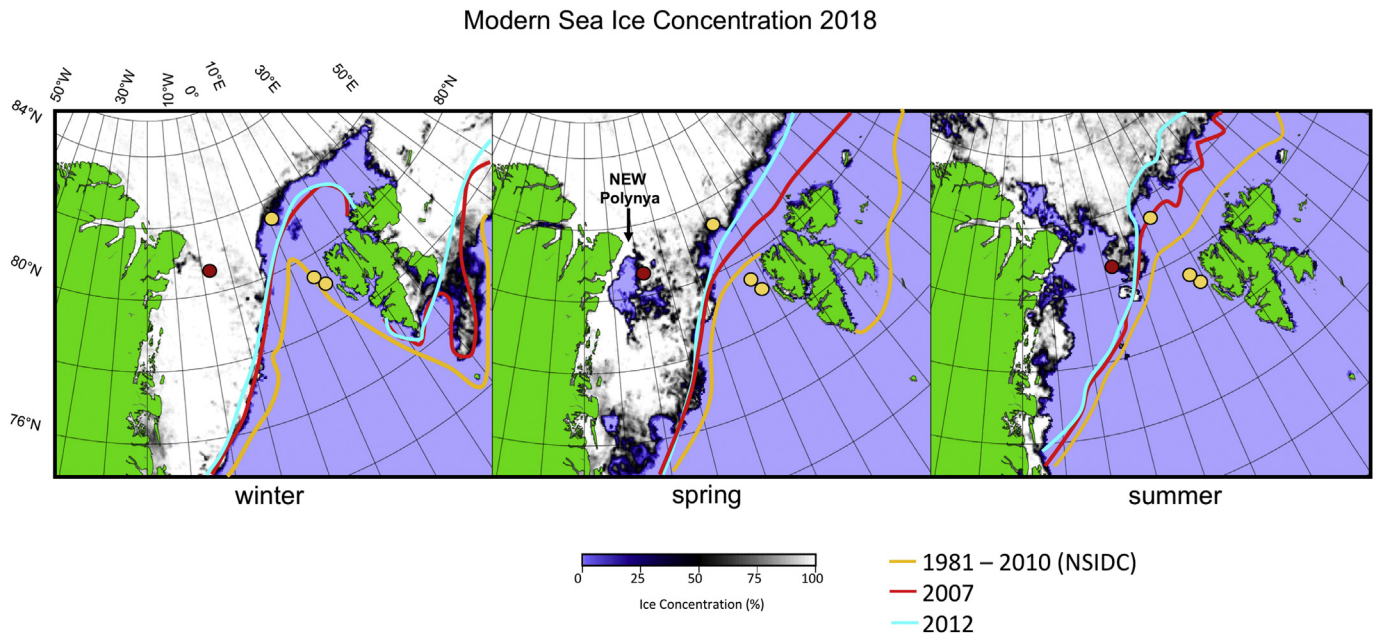

Fig. 1. Modern sea ice-concentration in the Fram Strait (Spreen et al., 2008; https://seaice.uni-bremen.de/databrowser/#p=sic, 2018). Closed sea ice cover during winter, seasonal opening of the Northeast-Water Polynya (NEW Polynya) during spring and strongly reduced sea ice during summer. Orange, red and blue lines showing the sea-ice extent from 1981 to 2010 and the extremely sea-ice reduced years 2007 and 2012 (NSIDC, Boulder.). Red dot shows the location of Core PS93/025, yellow dots the locations of other cores used in this study. (For interpretation of the references to color in this figure legend, the reader is referred to the Web version of this article.)

Greenland coastline in the west (Arndt et al., 2017; Fig. 2b and c). The knowledge about regional and local drivers of the sea-ice history and oceanic and atmospheric interactions on the eastern North Greenland continental shelf during the Holocene, however, remains fragmentary due to its low accessibility. Over the last years reduced sea-ice conditions have enabled a number of research expeditions into this area, allowing the recovery of sediment cores for detailed studies of paleoclimate and paleoceanographic

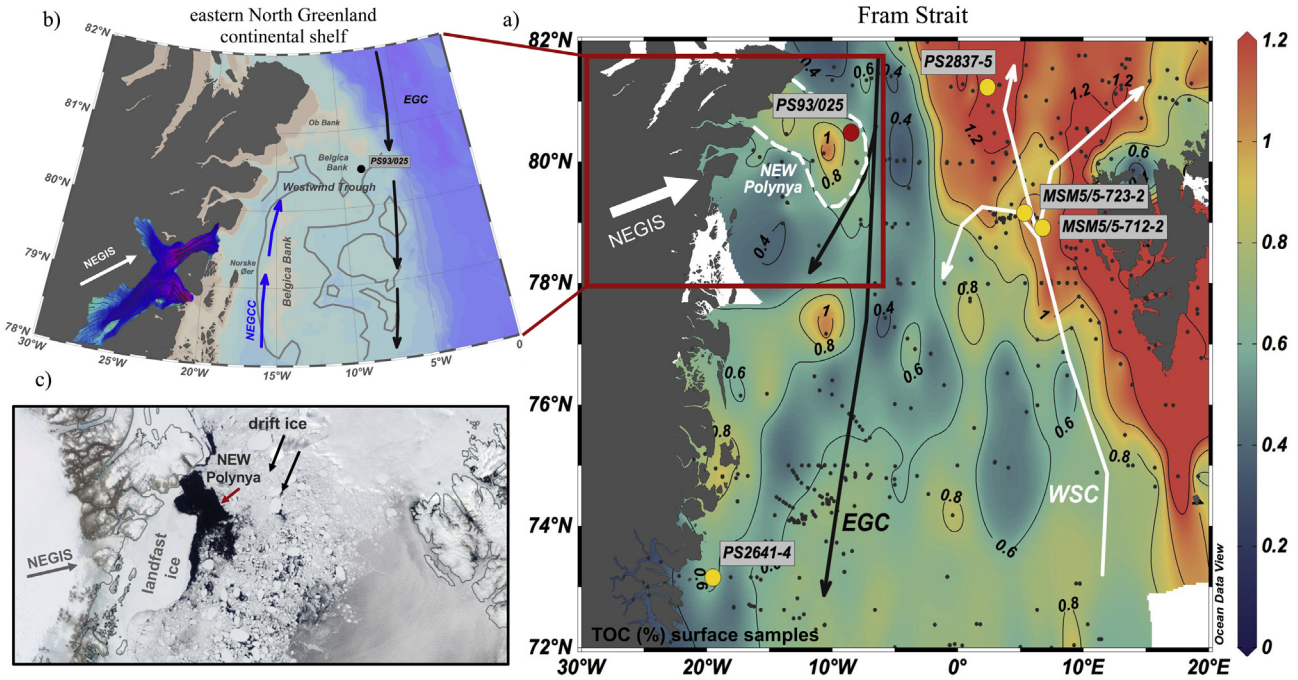

Fig. 2. a) Distribution of Total Organic Carbon (TOC) in surface sediments from the Norwegian-Greenland Sea and Fram Strait (Birgel and Stein, 2004; supplemented). Kastenlot Core PS93/025 (red circle) location at 80°N at the outer rim of the NEW Polynya (white dashed line, assumed area based on the TOC concentrations). Major surface ocean currents in the study area are the East Greenland Current (EGC, black arrows) and the West Spitsbergen Current (white arrows). Locations of further cores discussed in the text are marked as yellow circles. Northeast Greenland Ice Stream (NEGIS). b) Detailed map of the eastern North Greenland continental margin, including Core PS93/025 (black dot) taken from the upper edge of the Belgica Bank above the Westwind Trough, the southward flowing EGC (black arrow) and the northward flowing coastal Northeast Greenland Coastal Current (NEGCC, blue arrow). Norske Øer Ice Barrier is located in front of NEGIS. c) Satellite image (June 2019, credit: NASA Worldview: World Meteorological Organization, 1970) displaying outlet glaciers of NEGIS, landfast ice build-up along the coast, drift ice transported from the central Arctic Ocean and in between the seasonal formation of the NEW Polynya. (For interpretation of the references to color in this figure legend, the reader is referred to the Web version of this article.)

conditions. Furthermore, proxy-based methods for past sea-ice reconstructions have been further developed and applied within the Fram Strait and Arctic Ocean regions (e.g., de Vernal et al., 2013; Pieńkowski et al., 2016; Belt, 2018; Belt et al., 2019; Limoges et al., 2018).

The Holocene (0–11.7 ka), generally more climatically stable than the previous glacial transition (Grootes et al., 1993), was punctuated by rapid changes in climate and ocean dynamics (Mayewski et al., 2004; Sundqvist et al., 2014). In the Northern Hemisphere, the Holocene is roughly divided into three main intervals: (1) the early Holocene (~11.7–9 ka); (2) the mid Holocene (~9–5 ka) and (3) the late Holocene (~5–0 ka) (Briner et al., 2016; Renssen et al., 2006; Wanner et al., 2011). Especially, the late Holocene near-boundary conditions witnessed short-term alternations (<500 yrs), e.g. the Medieval Warm Period, Roman Warm Period and Little Ice Age (Ljungqvist, 2010). A declining solar insolation, freshwater influence, volcanic activity, and changes in the AMOC have been suggested as drivers for these short-term climate events (Andersen et al., 2004a, 2004b; Laskar et al., 2004; Rohling and Pälike, 2005; Renssen et al., 2006; Wanner et al., 2011). The Arctic Oscillation (AO) and North Atlantic Oscillation (NAO) regulate sea level pressure and the outflow of drift ice through the Fram Strait (Rigor et al., 2002), and significantly influence the weather and climate in the Northern Hemisphere on interannual-decadal timescales (Darby et al., 2012). Positive or negative AO/NAO modulations control the extensity of the Transpolar Drift system moving sea ice from Siberian shelves and the central Arctic Ocean in the direction of Greenland (Rigor et al., 2002; Bennike, 2004). So far, short-term variability of sea-ice extent is not sufficiently resolved in climate models, even though they have great relevance for predictions of the short-term variability in future climate (Loeb et al., 1997; Dieckmann and Hellmer, 2003; Funder et al., 2011).

This study utilizes biomarkers preserved in marine sediments from Core PS93/025, recovered from the outer eastern North Greenland shelf in the Northeast-Water Polynya (NEW Polynya, Fig. 1). This site is ideally suited to identify and disentangle the driving mechanisms of sea-ice distribution in the western Fram Strait. As proxies for the reconstruction of sea-ice cover we have used the sea-ice proxy IP_{25}, a highly branched isoprenoid (HBI) monoene with 25 carbon atoms (Belt et al., 2007), in combination with specific open-water phytoplankton and terrestrial higher land plant biomarkers (Müller et al., 2009; Stein et al., 2012; Belt and Müller, 2013; Belt et al., 2015, 2019; for further details see chapter 4.1). Based on these high-resolution biomarker data we are able to reconstruct sea-ice variability, primary productivity, terrigenous input and seasonal formation of the NEW Polynya that evolved during the Holocene at the eastern North Greenland shelf. Our results are compared with the eastern Fram Strait sea-ice trends.

1.2. Regional setting

The Fram Strait is the only deep-water connection between the Arctic and global oceans. Arctic Deep Water, filling the Fram Strait at depths greater than 800 m is overlain by Atlantic Intermediate Water (AIW) (Aagaard and Coachman, 1968a; Rudels and Quadfasel, 1991). The upper water layer is zonally divided by local surface ocean currents. On the eastern side of the Fram Strait relatively warm, saline Atlantic surface waters enter the Arctic Ocean via the West Spitsbergen Current (WSC, Fig. 2a). In contrast, the western Fram Strait is dominated by the outflow of cold Arctic surface waters of the East Greenland Current (EGC) (Aagaard and Coachman, 1968a, 1968b; Rudels et al., 1999). The low-saline EGC flows south along the eastern North Greenland shelf (Fig. 2a). These regional ocean currents result in a strong zonal surface temperature gradient. This zonal difference in sea-surface temperature causes a large disparity in sea-ice cover between the western and eastern Fram Strait. Consequently, west Spitsbergen is characterized by the northernmost ice-free water conditions during winter, while the sea-ice cover along the continental shelf off eastern North Greenland stretches much further south, due to regional sea-ice build-up and transport from the Arctic Ocean (Aagaard, 1982; Vinje, 1977). Sediments, drift ice and low-saline water masses formed on the Eurasian shelfs are transported via the Transpolar Drift across the central Arctic Ocean and eventually through the Fram Strait (Aagaard and Coachman, 1968a, 1968b; Eicken et al., 1995; Reimnitz et al., 1995; Schlichtholz and Houssais, 1999; Smedsrud et al., 2017).

Sea-ice conditions over the wide continental eastern North Greenland shelf in the western Fram Strait between 79 and 80° are additionally influenced by the waxing and waning of the ~700 km long Northeast Greenland Ice Stream (NEGIS), the largest ice stream in eastern North Greenland (Aagaard and Coachman, 1968b, Fig. 2b). This fast-flowing ice stream (20 m/year) drains 20% of the Greenland Ice Sheet and seasonally supplies large amounts of ice and freshwater to the eastern North Greenland shelf (Rignot and Kanagaratnam, 2006; Joughin et al., 2010; Rignot et al., 2011).

The coastal area north of NEGIS at ~80°N is characterized by the highly variable NEW Polynya (Fig. 1). Coastal polynyas are mostly ice-free areas surrounded by a denser sea-ice cover (Smith et al., 1990; WMO, 1985; Stirling, 1980). Northerly winds in combination with local ocean currents remove ice from the coastal region while grounding of icebergs and ice islands can prevent ice advection from the Arctic into the polynya region (Barber and Massom, 2007).

When the NEW Polynya opens up in April/May, reaching its final extension in summer, an anticyclonic circulation pattern appears over almost the entire ~300 km wide and shallow Belgica Bank with water depths ranging from 40 to 300 m (Bourke and Garrett, 1987; Kuklinski and Bader, 2007, Figs. 1 and 2c). A combined effect of a fast-ice barrier (the Norske Øer Ice Barrier), katabatic winds and a northward flowing North East Greenland Coastal Current (NEGCC) form the NEW Polynya (Fig. 2b, Schneider and Budéus, 1997). The water column in the NEW Polynya is characterized by AIW at the bottom overlain by Polar Water (PW) that circulates anticyclonic at the surface (Bourke and Garrett, 1987). Additionally, the surface waters in the polynya region are affected by melting of sea ice along the marginal ice zone and freshwater input from ice melting on land. The freshwater input from these processes stratifies the upper water column and fosters intense biological production until nutrients become depleted (Hirche et al., 1991; Schneider and Budéus, 1994; Budéus and Schneider, 1995). A significant ecosystem for primary producers (e.g., diatom blooms), marine mammals and seabirds is supported by the seasonally reduced ice cover of the recurring seasonal NEW Polynya (Stirling, 1980; Wadhams, 1981; Barber and Massom, 2007). Today, sea-ice cover varies from a dense sea-ice cover in winter to stable-ice-edge conditions during late spring/summer. This is also supported by elevated Total Organic Carbon (TOC) concentrations in sediments here, relative to surrounding areas (Fig. 2a; Birgel and Stein, 2004). However, understanding of the evolution and processes leading to polynya formation remain inconclusive.

2. Material and methods

2.1. Sediment material

Kastenlot Core PS93/025–2 was taken during RV Polarstern Cruise PS93.1 (2015) on the continental shelf off eastern North Greenland (80°28.90′N, 8°29.40′W) in 290.2 m water depth (Fig. 2a

and b, Stein, 2016). The coring location was selected based on detailed Hydrosweep and Parasound surveys. These surveys were used to identify small depressions with thick fillings of deglacial to Holocene sediments on the eastern North Greenland shelf, an area that is generally characterized by lag deposits due to strong bottom current activity. The recovered sediments consist of dark grayish brown, homogenous silty clay with relatively low magnetic susceptibility and wet bulk density values (Stein, 2016). Because of coring loss in the upper 25 cm of giant Kastenlot Core PS93/025−2, we correlate the uppermost part of the Kastenlot Core with a Box Core (GKG) PS93/025−1 covering the upper 43 cm of near surface sediments, based on the TOC content and spliced the records together at 27 cm to obtain a continuous and complete sedimentary record (named as Core PS93/025). From the Kastenlot and GKG cores, subcores were taken for multidisciplinary studies. One set of subcores devoted to biomarker analysis, was stored at −20 °C to prevent biomarker degradation.

2.2. Methods

2.2.1. Chronology

The age model is based on 19 accelerator mass spectrometry (AMS) ^{14}C ages measured on macro- and microfossil species, including benthic foraminifera (mixed species), planktic foraminifera (*Neogloboquadrina pachyderma*), bivalves, and scaphopods (not further identified) from GKG Core PS93/025−1 and Kastenlot Core PS93/025−2 (Table 1). AMS ^{14}C dating was carried out at the Alfred Wegener Institute Bremerhaven using the "Mini Carbon Dating System (MICADAS) and at the Leibniz-Laboratory in Kiel (Graphite Target). Radiocarbon ages were converted to calibrated calendar years before present (cal. years BP) using the calibration software CALIB 7.1 and the Marine13 calibration curve (Stuiver et al., 2019, Table 1). Five AMS ^{14}C ages at depths of 93.5 cm, 110.5 cm, 130.5 cm, 238 cm and 264 cm (Table 1, grey shaded areas) turned out to be reworked material within the sedimentary section and were therefore excluded. At a depth of 93.5 cm two AMS ^{14}C datings were performed on two different organism groups (bivalve and benthic foraminifera), but only one was used for the age model (Table 1).

Based on the radiocarbon ages we present two age models (Fig. 3). The first approach uses a 2nd order polynomial regression through the radiocarbon ages (see Zehnich et al., 2019). The second chronology is based on modeling by using the Bayesian R package B*chron* (Parnell et al., 2008) and the marine 13 calibration curve (Reimer et al., 2013). With the B*chron* model, two outliers at 62.5 and 125.5 cm would lead to extreme values up to 100 cm/kyr in the calculated sedimentation rate for which no evidence is found in the core data. We therefore excluded these two results from the Bayesian model. In the present study we have used the B*chron* age model for three reasons: Firstly, the Bayesian chronology remains within the error margin for the individual radiocarbon measurements; secondly, the 2nd order polynomial can only curve once, which may not fully reflect the variable nature of sediment input or flux under changing climatic conditions; thirdly, the Bayesian approach provides uncertainties and increases robustness of the age model. 10,000 age-depth realizations were obtained to estimate the median age and 95% confidence intervals at 1 cm resolution (Fig. 3). We acknowledge that application of the B*chron* age model results in a higher variability of calculated sedimentation rates and that a possible vertical displacement (from reworking or

Table 1
AMS^{14}C radio carbon ages for Kastenlot Core PS93/025 were determined on benthic and planktic foraminifers, bivalves and scaphopods. Bold CALIB median numbers were used for both age models (red ones were excluded in the B*chron* age model).

Lab-ID	Depth (cm)	Material	AMS ^{14}C	CALIB median	CALIB 2 sigma min	CALIB 2 sigma max
AWI 2053.1.1	15,5	Benth. foram.	926 ± 73	**540**	430	650
AWI 2054.1.1	42,5	Benth. foram.	1614 ± 75	**1170**	990	1300
AWI 2055.1.1	62,5	Benth. foram.	1816 ± 77	**1370**	1230	1540
KIA 52138	85,5	Bivalve	3225 ± 30	**3040**	2930	3150
KIA 51161*	93,5	Bivalve	3805 ± 25	3750	3660	3840
AWI 2056.1.1	93,5	Benth. foram.	3485 ± 84	**3370**	3150	3570
AWI 2057.1.1	106,5	Benth. foram.	3930 ± 81	**3920**	3690	4140
AWI 2058.1.1	125,5	Benth. foram.	4909 ± 89	**5220**	4960	5460
AWI 2059.1.1	141,5	Benth. foram.	5026 ± 83	**5380**	5190	5580
KIA 52139	110,5	Scaphopod	2521 ± 29	2200	2110	2290
BETA 445522*	130,5	Bivalve	3610 ± 30	3510	3410	3600
KIA 52140	163,5	Bivalve	5595 ± 35	**5980**	5900	6100
BETA 445523*	180,5	Bivalve	6340 ± 30	**6810**	6710	6900
KIA 52762	208	Plankt. foram.	7515 ± 45	**7970**	7870	8100
KIA 52763	217	Plankt. foram.	8055 ± 40	**8510**	8400	8600
KIA 52764	227	Plankt. foram.	8535 ± 40	**9170**	9020	9290
KIA 51162*	238	Scaphopod	8005 ± 35	8460	8380	8540
KIA 51162*	260	Bivalve	9380 ± 40	**10210**	10140	10330
KIA 52141	264	Bivalve	9250 ± 40	10080	9920	10180

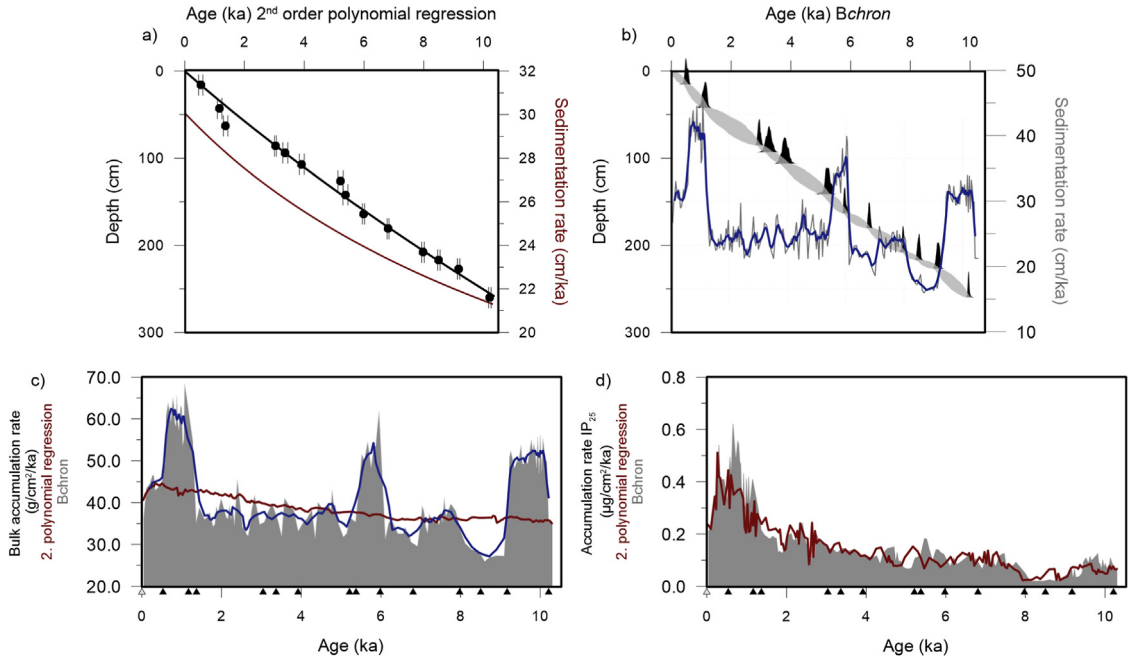

Fig. 3. a) Age model based on the 2. order polynomial regression with a relatively constant sedimentation rate (Zehnich et al., 2019). Black dots with error bars demonstrate measured corrected AMS ^{14}C ages for Core PS93/025 (Table 1). b) B*chron* age model (blue, bold line represents 5-point average, excluding two outliers at 62.5 and 125.5 cm, Table 1, Haslett and Parnell et al., 2008) used in this study, showing a variable sedimentation rate over the Holocene. c) Bulk accumulation rates based on 2. polynomial regression by Zehnich et al. (2019) (red line) and our B*chron* age model (blue line, grey shaded area with blue, bold line marking the 5-point average). d) Accumulation rates of IP_{25} emphasize similar trends of age models shown in a) and b). (For interpretation of the references to color in this figure legend, the reader is referred to the Web version of this article.)

bioturbation) of some of the dated materials cannot be ruled out. Nevertheless, the overall trends are very similar for both age models as shown, for example, in the IP_{25} accumulation rate records (Fig. 3). The sedimentation rates from the B*chron* age model range between 25 and 30 cm/kyr over the past 10.2 ka, except for three intervals of high sedimentation rates (up to ~40–45 cm/kyr) between 0.8 and 1.1 ka, 5.7–6 ka and 9–10 ka (Fig. 3).

2.2.2. Organic bulk sediment parameters

Total organic carbon (TOC), total carbon (TC) and total nitrogen (TN) were measured using freeze-dried and homogenized bulk sediment samples in intervals of 1 cm. TOC measurements were performed with a Carbon–Sulfur Analyser (CS-125, Leco) after removing any carbonate by adding hydrochloric acid to a 0.1 g subsample. TC and TN contents were measured on sediment samples of 20 mg sediment with a Carbon–Nitrogen–Sulfur Analyser (Elementar III, Vario). Subsequently, the carbonate content ($CaCO_3$) was calculated from TOC and TC ($CaCO_3$=(TC-TOC) x 8.333), assuming that carbonate predominantly occurs in the form of calcite, where 8.333 is the stoichiometric calculation factor. The TOC vs. total nitrogen (C/N) ratio may give some first-order information about the organic-carbon source, with higher/lower values more indicative for a terrigenous/marine origin (for details and limitations of this approach see Stein and Macdonald, 2004).

2.2.3. Extraction and analysis of lipid biomarkers

Specific highly branched isoprenoids, so called HBIs, (IP_{25}, HBI diene (HBI II) and HBI z-triene (HBI III)) and the sterols brassicasterol (24-methylcholesta-5,22-dien-3β-ol), dinosterol (4α,23,24-Trimethyl-5α-cholest-22E-en-3β-ol), β-sitosterol (24-ethylcholest-5-en-3β-ol) and campesterol (24-methylcholest-5en-3β-ol)) were extracted and analyzed. 5 g of freeze-dried and homogenized sediment were extracted in intervals between 1 and 3 cm. For the extraction, dichloromethane/methanol (DCM/MeOH, 2:1 v/v) was added to the sediment samples additionally with the internal standards 7-hexylnonadecane (7-HND, 0.076 µg/sample), 9-octylheptadec-8-ene (9-OHD, 0.1 µg/sample), 5α-androstan-3β-ol (androstanol, 10.7 µg/sample) and squalane (3.2 µg/sample) for the quantification of lipid biomarkers in each sample, followed by ultrasonification (15 min) and centrifugation (3 min) three times. Subsequently, we separated the hydrocarbon fraction (5 ml *n*-hexane) from the sterol fraction (9 ml ethylacetate/*n*-hexane) by open silica gel column chromatography. Finally, the sterol fraction was silylated by adding 200 µl of BSTFA (bis-trimethylsilyl-trifluoroacet-amide) at 60 °C for 2 h. Two different gas chromatography-mass spectrometers (GC-MS) with similar basic configuration were used to measure the extracted samples. The hydrocarbon fraction was measured with a gas chromatograph Agilent Technologies 7890B GC system (30m DB-1MS column, 0.25 mm i.d., 0.25 µm film thickness) coupled to a mass spectrometer Agilent 5977A MSD (70 eV constant ionization potential, Scan 50–550 m/z, 1 scan/s, ion source temperature 230 °C, Performance Turbo Pump) with the temperature program: 60 °C (3 min), 150 °C (heating rate: 15 °C/min), 320 °C (heating rate: 10 °C/min) and 320 °C (15 min, isothermal). The sterols were measured with a GC Agilent 6850 GC coupled to an Agilent 5975C VL MSD (conditions see above) with the temperature sequence: 60 °C (2 min), then 150 °C (heating rate: 15 °C/min), 320 °C (heating rate: 3 °C/min) and 320 °C (20 min isothermal).

Component assignment was based on comparison of GC retention times with those of reference compounds and published mass spectra (sterols: Boon et al., 1979; Volkman, 1986; HBIs: Belt et al., 2007; Brown and Belt, 2016). The concentration of each biomarker was calculated by setting its individual GC-MS ion responses in relation to those of respective internal standards. For the quantification of the sterols (quantified as trimethylsilyl ethers), the molecular ions *m/z* 470 for brassicasterol, *m/z* 472 for campesterol, *m/z* 486 for β-sitosterol, and *m/z* 500 for dinosterol were used in

relation to the molecular ion *m/z* 348 of the internal standard androstanol. For the quantification of IP_{25}, HBI II and HBI III, their molecular ions (*m/z* 350 for IP_{25}, *m/z* 348 for HBI II, and *m/z* 346 for HBI III) were compared to the fragment ion *m/z* 266 of the internal standard 7-HND. The different responses of these ions were balanced by an external calibration. For further details we refer to Fahl and Stein (2012), Brown et al. (2014) and Belt (2018).

The calculated Kovats Index for IP_{25} is 2085, for HBI II 2084 and 2046 for HBI III. All biomarkers of this study were normalized against the amount of sediment and TOC content.

We calculated the PIP_{25} indices according to the equation by Müller et al. (2011), where c is a concentration balance factor (to account for concentration differences between IP_{25} and phytoplankton biomarkers (P), i.e., brassicasterol, dinosterol or HBI III:

$$(1)\quad PIP_{25} = \frac{[IP_{25}]}{([IP_{25}] + c[P])} \quad \text{with} \quad c = \frac{\text{mean}[IP_{25}]}{\text{mean}[P]}$$

On average, concentrations of brassicasterol are about five times higher, dinosterol about ten times higher and HBI III about two times lower than the IP_{25} concentrations in Core PS93/025, resulting in balance factors of 0.23, 0.11 and 2.44, respectively.

Biomarker concentrations were converted into accumulation rates by using the following equations (e.g. Stein and Macdonald, 2004):

$$(1)\quad \text{Porosity}\ \ PO(\%) = \frac{(GD - WBD)}{GD - 1.026} * 100$$

$$(2)\quad TS - AR\left(g\ cm^{-2} ky^{-1}\right) = LSR * (WBD - 1.026\ PO/100)$$

$$(3)\quad OC - AR\left(g\ C\ cm^{-2} ky^{-1}\right) = TS - AR * OC \Big/ 100$$

GD = grain density of 2.65g cm^{-3} $\quad WBD$ = wet bulk density(g/ccm)

LSR = sedimentation rate(cm/ka) $\quad TS$ = *total* sediment

OC = total organic carbon(%) $\quad BM$ = biomarker concentration$\left(\mu g\ g^{-1} Sed\right)$

2.2.4. Statistical analyses

Significant shifts in biomarker records of Core PS93/025 (Fig. 4) were identified using the changepoint analysis from the R package ECP with a significance level of 99% (James and Matteson, 2013; R Core Team, 2018). The variability of average HBI and sterol concentrations of the five intervals defined in the Holocene record of Core PS93/025 is shown in Fig. 5.

For spectral analysis, IP_{25}, brassicasterol and HBI III time series were resampled at 0.03 kyr resolution prior to spectral analysis. Then spectral analysis was carried out using the multitaper method (MTM) with three 2π tapers (Thomson, 1982) and LOWSPEC noise estimation as implemented in the R package „astrochron" (Meyers, 2012). Confidence levels were calculated by applying the LOWESS-based (Cleveland, 1979) procedure of Ruckstuhl et al. (2001).

3. Results

3.1. Organic/inorganic bulk parameters

In the following, data are presented versus age. Single records of the bulk parameters versus depth are available in the supplementary material S1. The TOC record of Core PS93/025 can be divided into three intervals with low values of 0.5–0.6% between 10.2 and 7.9 ka, constant values of ~0.6% from 7.9 to 5.1 ka and increasing values from 5.1 ka towards the top, reaching 0.8–0.9% in the last 1 ka (Fig. 4). High C/N ratios of 7.5–9 occur in the lower part of the core between 10.2 and 8.8 ka whereas lower values between about 6 and 7.5 are typical for the interval from 8.8 ka onwards (Fig. 4). Maximum inorganic carbon (IC) values of 0.8–1.0% (i.e., 7–8.5% $CaCO_3$) were determined in the lower part between 10.2 and 7.9 ka. After 7.9 ka, IC values sharply decrease, and values of 0.55–0.65% (i.e., 4.5–5.5% $CaCO_3$) are typical for the interval between 7.9 and 5.5 ka. In the upper part of the core between 5.5 ka and the top, IC values vary between 0.35 and 0.65% (i.e., 3–5.5% $CaCO_3$), with higher values of 0.6–0.65% (i.e., 5–5.5% $CaCO_3$) most dominant in the interval between 1.3 and 0.6 ka (Fig. 4).

3.2. Biomarker

Results of all biomarker records are plotted in μg g^{-1} TOC and as accumulation rates in μg cm^{-2} ky^{-1} versus age (Fig. 4). In addition, each biomarker is plotted in μg g^{-1} Sed and μg g^{-1} TOC versus depth, presented in the supplementary material S2. Due to the good correlation of campesterol and β-sitosterol, both records were combined into one record of terrigenous biomarkers that is used in the discussion. The sterols (brassicasterol, dinosterol, campesterol and β-sitosterol) of Core PS93/025 vary more or less synchronously over the entire Holocene record, which can be subdivided into three main intervals (Fig. 4). High concentrations of the phytoplankton biomarkers brassicasterol (4–6 μg g^{-1} TOC) and dinosterol (~8–10 μg g^{-1} TOC) and the terrigenous biomarkers campesterol and β-sitosterol (both ~13 μg g^{-1} TOC) occur between 10.2 and 9.3 ka. Relatively stable, but low values of brassicasterol (~2 μg g^{-1} TOC), dinosterol (~4 μg g^{-1} TOC), campesterol and β-sitosterol (~5 μg g^{-1} TOC), are obvious between 9.3 and 1 ka. During the last 1 ka, all sterols reach maximum values with brassicasterol (up to 8 μg g^{-1} TOC), dinosterol (up to 15.5 μg g^{-1} TOC), campesterol and β-sitosterol (both up to 22.5 μg g^{-1} TOC) (Fig. 4).

The IP_{25} record can also be subdivided into three intervals. Low IP_{25} values of 0.4 μg g^{-1} TOC characterize the interval between 10.2 and 7.9 ka, while slightly higher values of ~0.6 μg g^{-1} TOC were found between 7.9 and 4.8 ka (Fig. 4). From 4.8 ka onwards, the IP_{25} concentrations increase continuously, reaching maximum values of 1.4 μg g^{-1} TOC during the last 1 ka (Fig. 4). The HBI III record was divided into five intervals. High HBI III concentrations occur from 10.2 to 9.3 ka (values up to ~0.6 μg g^{-1} TOC), between 7.9 and 5.5 ka (up to 0.4 μg g^{-1} TOC) and during the last 1 ka (up to 0.8 μg g^{-1} TOC), intercalated by intervals of lower concentrations between 9.3 and 7.9 and 5.5 and 1 ka with values below 0.1 μg g^{-1} TOC (Fig. 4).

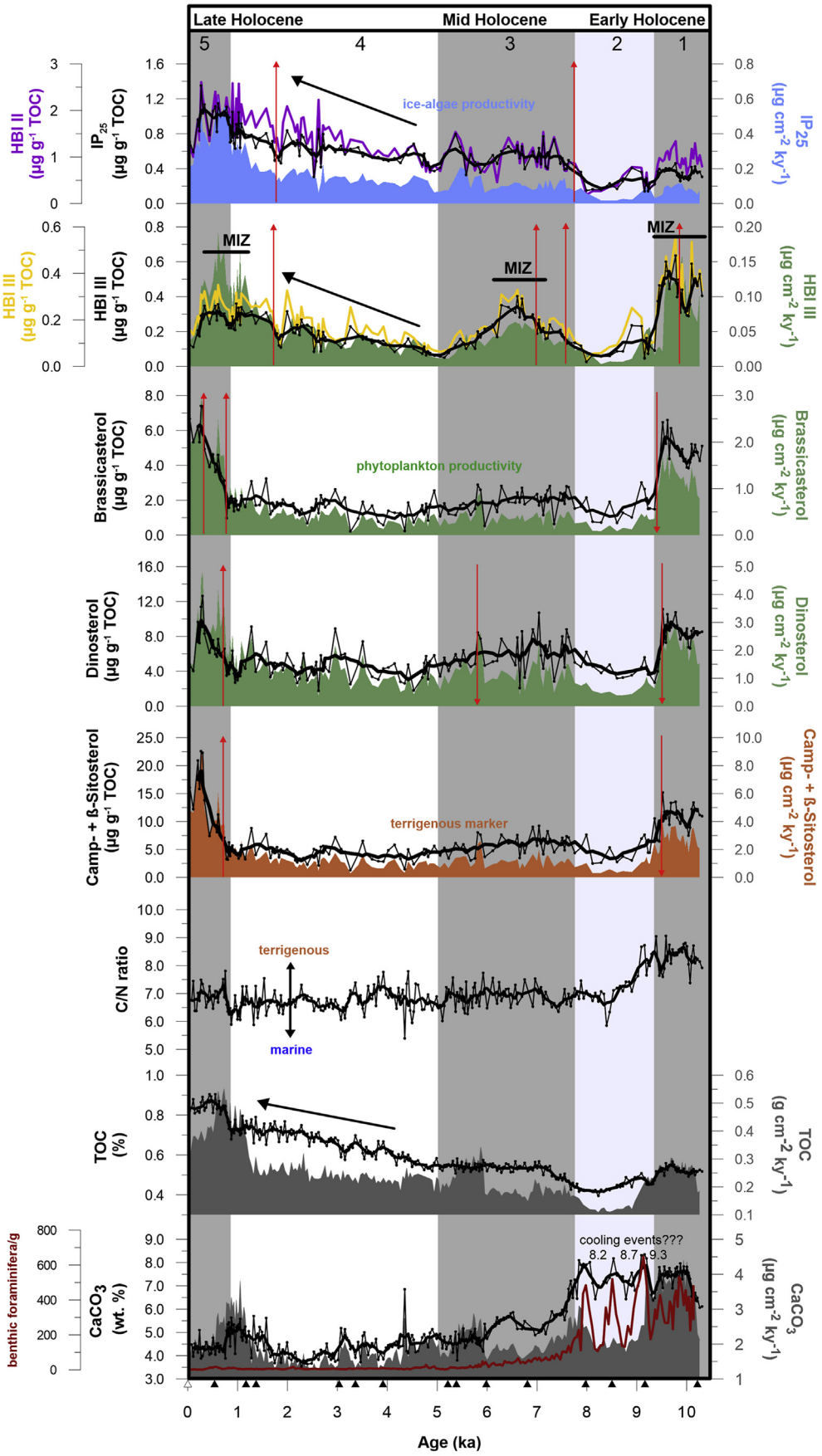
Late Holocene
Mid Holocene
Early Holocene
5
4
3
2
1
HBI II (µg g-1 TOC)
IP25 (µg g-1 TOC)
ice-algae productivity
IP25 (µg cm-2 ky-1)
HBI III (µg g-1 TOC)
MIZ
MIZ
MIZ
HBI III (µg cm-2 ky-1)
Brassicasterol (µg g-1 TOC)
phytoplankton productivity
Brassicasterol (µg cm-2 ky-1)
Dinosterol (µg g-1 TOC)
Dinosterol (µg cm-2 ky-1)
Camp- + ß-Sitosterol (µg g-1 TOC)
terrigenous marker
Camp- + ß-Sitosterol (µg cm-2 ky-1)
C/N ratio
terrigenous
marine
TOC (%)
TOC (g cm-2 ky-1)
benthic foraminifera/g
CaCO3 (wt. %)
cooling events???
8.2
8.7
9.3
CaCO3 (µg cm-2 ky-1)
Age (ka)

Overall, accumulation rates of all biomarkers reflect similar trends during the Holocene.

4. Discussion

4.1. Proxies used for past sea-ice reconstructions on the eastern North Greenland shelf: some general aspects

In this study past sea-ice reconstructions on the eastern North Greenland shelf were carried out by using the sea-ice proxy IP_{25} (Belt et al., 2007) in combination with the tri-unsaturated HBI (HBI III, phytoplankton biomarker) and specific sterols (phytoplankton and terrigenous biomarkers). IP_{25} is produced by diatoms that inhabit the sea ice with highest concentrations during spring algae blooms (Belt et al., 2007; Brown et al., 2014, 2016). Thus, IP_{25} is a reliable and direct indicator for past seasonal sea-ice presence. Sediment traps studies evidence the release of ice algal organic carbon (OC) containing the IP_{25} signal, that sinks to the ocean surface during the ice melt (Belt et al., 2008; Fahl and Stein, 2012). Over the past years, IP_{25} has been successfully used to reconstruct sea-ice variability across the Arctic (for reviews see Stein et al., 2012; Belt and Müller, 2013; Belt, 2018) even in regions with a near-permanent sea-ice cover (Xiao et al., 2015). However, this proxy has a few limitations (Belt, 2018). Sea-ice algae are absent in ice-free areas but also absent or only occur in very minor amount in areas characterized by a more closed and thick sea-ice cover that prevents significant algae productivity. Thus, IP_{25} is not found or only found in very minor amount in the underlying sediments. Additionally, several other factors may hamper the IP_{25} production and accumulation, for example lower salinities in fjords or near-coastal surface waters due to large river input or meltwater discharge (Xiao et al., 2013; Hörner et al., 2016; Ribeiro et al., 2017), or brine channels within the sea ice, or reduced light availability through an overlying snow cover (Belt and Müller, 2013). Lately, the discussion about degradation of IP_{25} in terms of ice-algal carbon as foodstock (grazing) within the water column, and oxidation of IP_{25} within the sea ice, has received greater awareness (for details see Belt, 2018). Another substitutional sea-ice proxy (biosynthesized by Arctic diatoms) and often very well correlated with IP_{25}, might be the HBI II diene (Brown et al., 2014), with concentrations often somewhat higher than those of the IP_{25} (for details see Belt, 2018).

IP_{25} in combination with open-water phytoplankton biomarkers allows a more detailed classification of sea-ice conditions. As open-water phytoplankton biomarkers Müller et al. (2009, 2011) originally used specific sterols (brassicasterol, dinosterol), and proposed a combined phytoplankton-IP_{25} proxy (PIP_{25}) that allows a more semi-quantitative description of spring sea-ice conditions (for PIP_{25} calculations see subchapter 2.2.3; for general information about methods and interpretation of the approach see Müller et al., 2011; Belt et al., 2015; Smik et al., 2016). According to Müller et al. (2011), sea-ice conditions were classified into ice-free conditions ($PIP_{25} = 0$), a low to variable sea-ice cover ($PIP_{25} > 0.1$) with low IP_{25} and high phytoplankton biomarker values, the marginal ice zone ($PIP_{25} > 0.5$) with intermediate values and extended sea-ice conditions ($PIP_{25} > 0.75$) with high IP_{25} and low phytoplankton biomarker values. A perennial closed sea-ice cover would result in IP_{25} and phytoplankton biomarker concentrations near zero, i.e. PIP_{25} would become indeterminable and thus often artificially set to 1. These extreme values, however, have to be interpreted with caution and the single biomarker concentrations should be considered as well (cf., Stein et al., 2017; Belt, 2018). Furthermore, the degree of accuracy of PIP_{25} may depend on the combination of specific phytoplankton biomarkers (and their pelagic origin), the c balance factor (c.f. subchapter 2.2.3), the algorithmic relationship between the PIP_{25} and the different sea-ice conditions, as well as the temporal shifts within the downcore records (Belt, 2018).

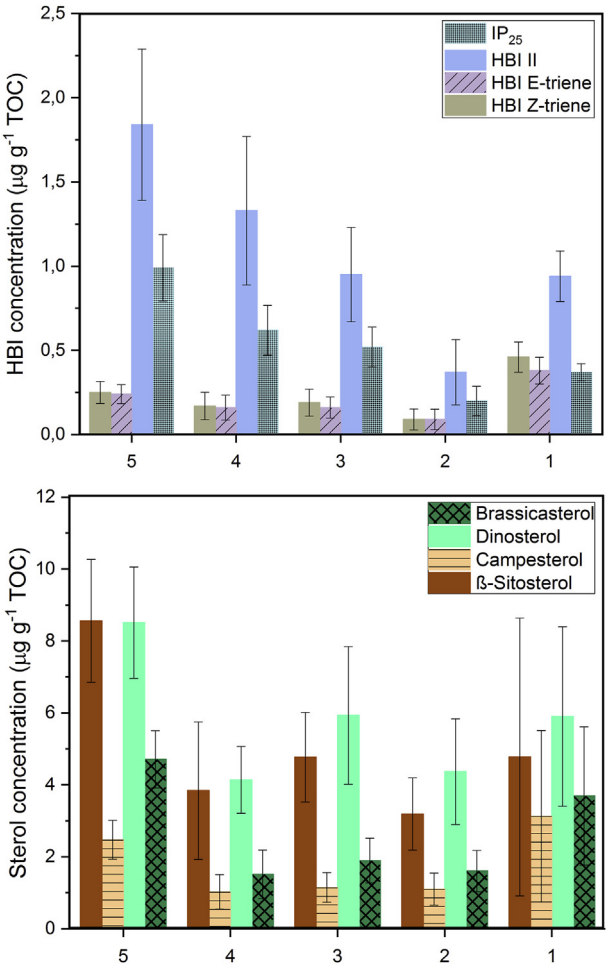

Fig. 5. Average of the HBI and sterol concentrations with error bars (±1 sample SD in each case) for the defined five time intervals of our Holocene record (cf., Fig. 4).

More recently, the HBI III triene (e and z triene) has been used as a complimentary proxy to IP_{25}. HBI III is probably an indicator for pelagic diatom productivity of the species *Rhizosolenia setigera* in the photic zone of the water column, and is strongly associated in (sub-) polar regions with the Marginal Ice Zone (MIZ) (Collins et al., 2013; Smik et al., 2016; Belt, 2018). The consideration of ice-associated IP_{25} and HBI II alongside with the pelagic HBI III triene (e and z triene) might help to distinguish between different sea-ice scenarios (see Belt, 2018). Positively correlated IP_{25} and HBI III profiles were assumed to reflect rapidly changing (advancing/retreating) sea-ice margins or offshore polynyas (cf., Belt, 2018) and negatively correlated profiles are attributed to temporal shifts in the winter/summer sea-ice margin (Belt et al., 2015; Berben et al., 2017). Furthermore, different interpretations of the proxy data might be possible when using this approach in different regions.

Fig. 4. Organic bulk parameters (TOC, $CaCO_3$ and C/N ratio), planktic foraminiferal counts (red curve, Zehnich et al., 2019), biomarker concentrations (left) and accumulation rates (right, coloured shaded curves) of Core PS93/025. Thick black line shows 5-point average trend. Significant shifts within the biomarker records are indicated by red arrows and based on the change-point analyses with a confidence level of 99.5%. Grey bars separate five intervals of climate changes during the Holocene discussed in the text. Black triangles mark corrected AMS ^{14}C-dated core depths. (For interpretation of the references to color in this figure legend, the reader is referred to the Web version of this article.)

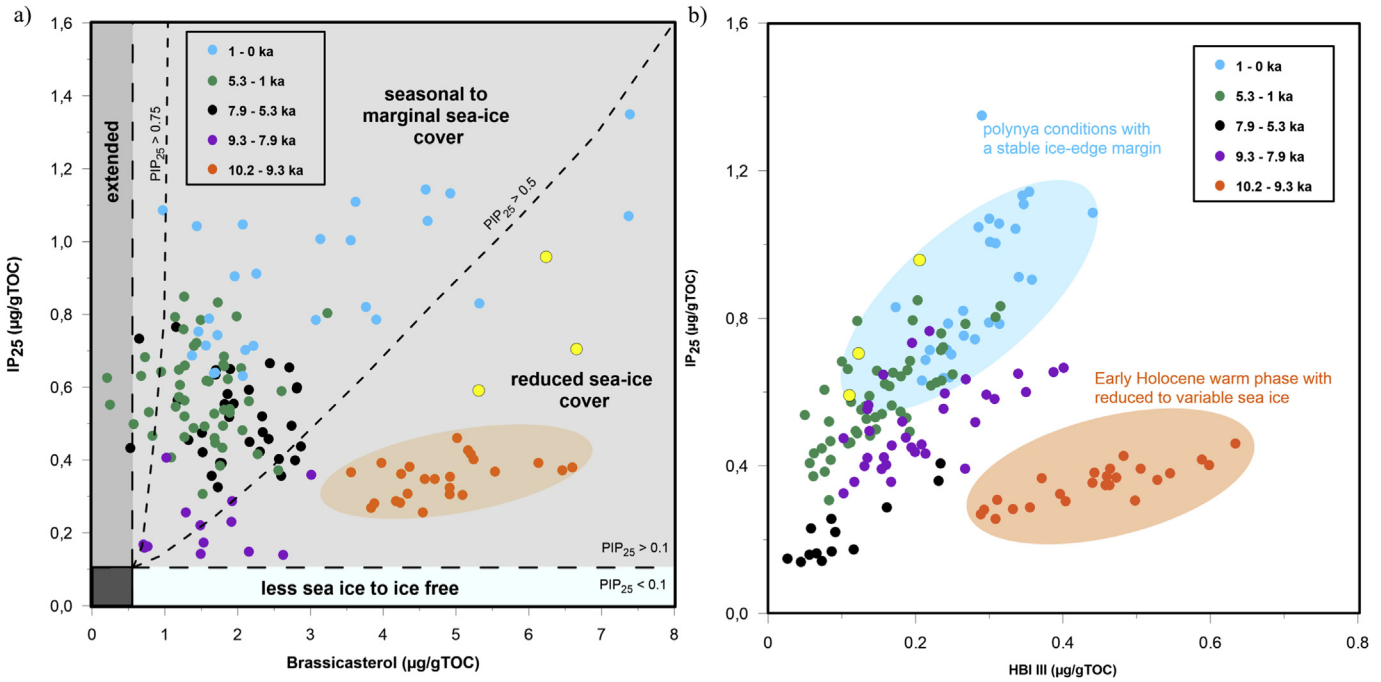

Fig. 6. a) Scatter plot (µg g^{-1} TOC) of IP_{25} versus brassicasterol with different sea-ice scenarios after Müller et al. (2011). b) scatter plot (µg g^{-1} TOC) IP_{25} versus HBI III of Core PS93/025-2 highlighting the early Holocene warm phase (orange shaded area) and the assumed seasonal formation of the NEW polynya during the last 1 ka (blue shaded area). Data from the five Holocene intervals are indicated by different colors. The yellow circles mark data from the uppermost 1-6 cm of Core PS93/025, probably representing modern-type conditions. (For interpretation of the references to color in this figure legend, the reader is referred to the Web version of this article.)

For example, based on data of surface sediments from the Barents Sea and around Svalbard, Smik et al. (2016) concluded that the HBI III triene in combination with IP_{25} ($P_{III}IP_{25}$) is a promising indicator for winter sea-ice extent and/or the MIZ. Findings from eastern North Greenland fjord surface sediment samples seem to support this statement since HBI III concentrations were also found to be most abundant in locations proximal to the ice edge (Ribeiro et al., 2017). In contrast to the Barents Sea area, however, the HBI maximum concentrations correlate with the mid-July MIZ in the Greenland fjord area that is characterized by much heavier sea-ice conditions in general.

To identify terrigenous organic carbon, we have used specific sterols (β-sitosterol and campesterol), C/N ratios and TOC values. For further details of the identification of organic carbon sources see Stein and Macdonald (2004); Fahl and Stein (1999, 2012) and Belt (2018).

In summary, multivariate analysis of individual open-water phytoplankton and terrigenous biomarkers in combination with IP_{25} and PIP_{25} records may help to identify different sea-ice scenarios and organic carbon source areas (marine vs. freshwater) (see Fig. 6 and suppl. mat. S3).

4.2. Sea-ice variability off eastern North Greenland during the Holocene

4.2.1. Early Holocene (10.2–7.9 ka)

During the late Holocene between 10.2 and 9.3 ka, low IP_{25} and HBI II fluxes reflect reduced to moderate sea-ice algae productivity, while considerably high phytoplankton biomarker concentrations and fluxes of brassicasterol, dinosterol and HBI III (Fig. 4) indicate prolonged open-water conditions with enhanced biological productivity at the outer eastern North Greenland continental shelf. Such a reduced sea-ice situation is also clearly reflected in the related minimum P_BIP_{25}, P_DIP_{25} and $P_{III}IP_{25}$ indices of <0.3 (Fig. 7) and the scatter plot of IP_{25} indices against the phytoplankton biomarker brassicasterol and HBI III (Fig. 6). Considering the generally reduced sea-ice conditions and the distinct HBI III maximum, this may represent a winter MIZ situation (Fig. 4, interval 1) as proposed by Belt et al. (2015) for the modern Barents Sea. Strongly reduced sea-ice conditions were also reconstructed for the inner East Greenland shelf (Core PS2641-4) and the eastern Fram Strait (MSM5/5-712-2 and MSM5/5-723-2) during the early Holocene based on relatively high phytoplankton biomarker values, high $CaCO_3$ and lowered IP_{25} and IRD contents (Müller et al., 2012). The eastern Fram Strait sea-ice conditions during the early Holocene most likely correspond to the present-day summer situation (cf., Fig. 1c).

The low sea-ice coverage and relatively warm surface water conditions due to the intensified inflow of warmer recirculating Atlantic Water from the eastern towards the western Fram Strait (Koç et al., 1993; cf. Carstens et al., 1997; Volkmann, 2000; Pados and Spielhagen, 2014), favored planktic blooms at our core site, as reflected by elevated numbers of planktic and benthic foraminifers and highest (biogenic) $CaCO_3$ content and flux (Fig. 4). Warmer sea-surface conditions were also reconstructed for the Nordic Seas and the East Greenland shelf based on foraminifers and diatoms (Bauch et al., 2001; Andersen et al., 2004a, 2004b). The appearance of *Armeria scabra* and the sub-arctic mussel *Mytilus edulis*, both species are well-known for their occurrence in eastern North Greenland, further support warmer summer temperatures than today during the early Holocene between 10 and 8.5 ka (Hjort and Funder, 1974; Bennike and Weidick, 2001).

During this warmer early Holocene period, elevated fluxes of terrigenous organic matter indicated by high β-sitosterol and campesterol values and high C/N ratios (Fig. 4), and the decrease of IRD deposition (Telesiński et al., 2014; Zehnich et al., 2019) may have resulted from melting by local glaciers from eastern North Greenland and related meltwater discharge (cf., Blaschek and

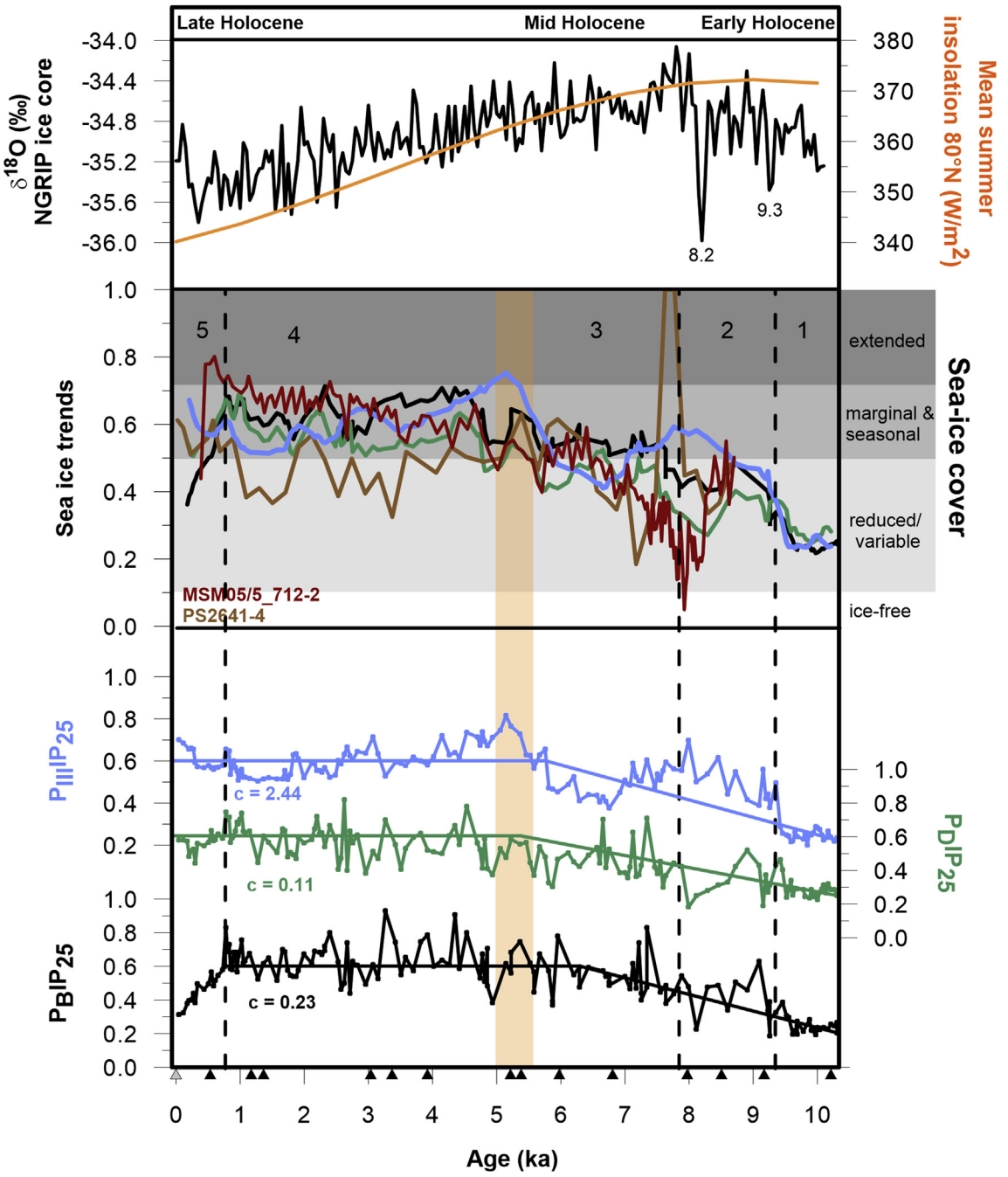

Fig. 7. P_BIP_{25} (black line), P_DIP_{25} (green line) and $P_{III}IP_{25}$ (blue line) records of Core PS93/025. Upper part displays Holocene sea-ice trends with additional data (calculated with brassicasterol as phytoplankton) from the eastern Fram Strait (MSM5/5-712-2; Müller et al., 2012), East Greenland continental shelf (PS2641-4; Müller et al., 2012) and this study (PS93/025). Black triangles mark corrected AMS ^{14}C-dated core depths. $\delta^{18}O$ values of the NGRIP ice core (NGRIP-Members, 2004) and summer insolation (orange curve; Laskar et al., 2004) show the Holocene cooling trend. (For interpretation of the references to color in this figure legend, the reader is referred to the Web version of this article.)

Renssen, 2013). This may have provided nutrient-rich freshwater to the eastern North Greenland shelf causing stratification of the surface layer and intensified phytoplankton growth (Waniek et al., 2005). This explanation would also explain the high positive correlation between the phytoplankton (i.e., brassicasterol and dinosterol) and the terrigenous biomarkers (β-sitosterol and campesterol) (suppl. material S3).

In summary, our data of Core PS93/025 and multiproxy records (e.g., IRD, $\delta^{18}O$, $\delta^{13}C$, benthic and planktic foraminifera abundances) from other nearby cores (Telesiński et al., 2014) relate the phase between 10.2 and 9.3 ka to be linked to the Holocene Thermal Maximum (HTM), where increased mean local summer insolation led to summer temperatures 4–5 °C warmer than today in northern Greenland (Kaufman et al., 2004; Laskar et al., 2004; Reeh, 2004; Lecavalier et al., 2017).

Around 9.3 ka a prominent change in environmental conditions occurred, as reflected in a significant shift from high to low concentrations and accumulation rates of all biomarkers (Figs. 4 and 5) suggesting reduced sea-ice and open-water algal productivity. This change may be related to an extended sea-ice cover as shown in the elevated PIP_{25} indices (Fig. 7). Superimposed to this change towards an increased sea-ice cover, three distinct maxima and minima in

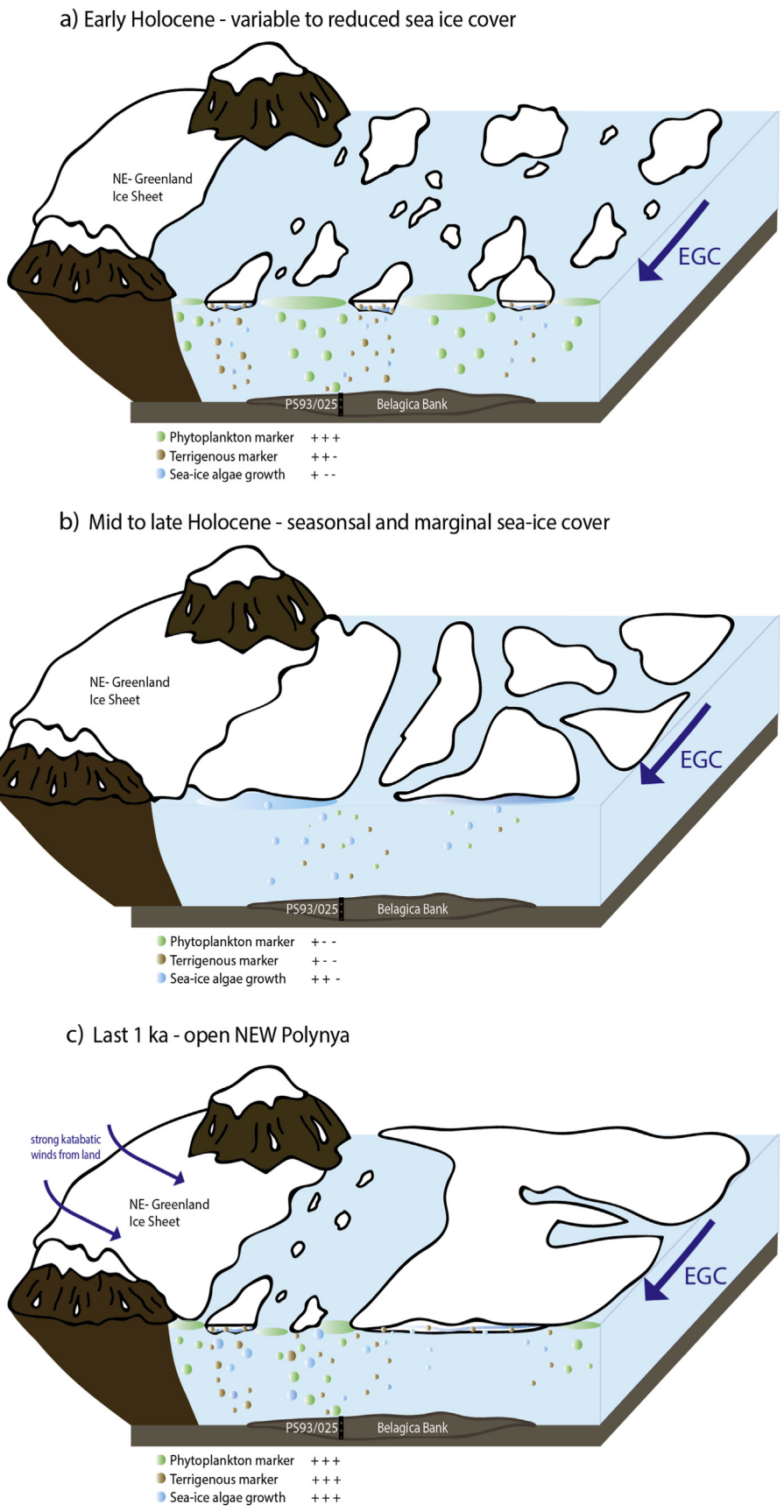

Fig. 8. Schematic illustration of sea-ice variability on the eastern North Greenland shelf during the a) early Holocene b) mid to late Holocene and c) the last 1 ka. Variations of each biomarker production is characterized by coloured dots and patches (blue: sea-ice algae, green: phytoplankton and brown: terrigenous marker). Core location PS93/025 is highly influenced by the NEGIS, the EGC, and the NEW Polynya. (For interpretation of the references to color in this figure legend, the reader is referred to the Web version of this article.)

the higher-resolution carbonate concentration and planktic foraminifer are obvious, implying short-term disturbances in sea-surface conditions (Fig. 4). A reasonable explanation for these disturbances might be short-lived small cooling events, similar to the 8.2 Event (Kobashi et al., 2007; Rasmussen et al., 2007; Thomas et al., 2007), which was probably triggered by freshwater outbursts from the Laurentide Ice Sheet-dammed lakes into the North Atlantic Ocean and had a considerable impact on the thermohaline circulation (Barber et al., 1999; Yu et al., 2010). Thus, the minima in our records (Fig. 4) between 7.9 and 9.3 ka may reflect increased sea-ice conditions and strongly reduced phytoplankton productivity due to abrupt freshwater outbursts.

4.2.2. Mid Holocene (7.9–4.9 ka)

Elevated IP_{25} and HBI II values, but overall low and stable (with minor fluctuations) phytoplankton biomarker (brassicasterol and dinosterol) and terrigenous biomarker concentrations and accumulation rates revealed during the mid Holocene (Fig. 4). Rising PIP_{25} indices indicate a gradual transition from reduced to seasonal sea-ice conditions along the outer eastern North Greenland continental shelf (Fig. 8b). Contemporaneously, decreasing $CaCO_3$ concentrations and relatively low abundances of foraminifers (Zehnich et al., 2019) occur during the same interval. In fact, a decreasing warm Atlantic Water advection may have caused a gradual cooling evidenced by lowered SSTs in the Fram Strait (Bauch et al., 2001; Jennings et al., 2002; Müller et al., 2012) and constantly reduced phytoplankton productivity at Core PS93/025. Meanwhile, increased abundances of Arctic diatom taxa point to a strengthened EGC between 6.8 and 5.5 ka (Ran et al., 2006) that would have transported more sea ice (drift ice) from the Arctic along the eastern North and East Greenland shelf southward towards Iceland (Andrews et al., 2009; Cabedo-Sanz et al., 2016).

Maximum concentration and flux of HBI III (Fig. 4) might indicate the build-up of a stable MIZ in the interval between about 7 and 6 ka. Following Ribeiro et al. (2017) and their study of surface sediments from the eastern North Greenland shelf, this probably represents a (spring) summer MIZ situation (Fig. 4, interval 3).

4.2.3. The late Holocene (5–1 ka)

During the late Holocene, the three PIP_{25} indices do not show any trend, but fluctuate around 0.6 (Fig. 7). These values represent typical seasonal to marginal sea-ice conditions. The ice-associated IP_{25} and HBI II records only display a minor increase between 5 and 1 ka (Figs. 4 and 5). This is in contrast to several IP_{25} records from other Arctic regions, including the Yermak Plateau (Müller et al., 2009), north of Iceland (Cabedo-Sanz and Belt, 2016) and Spitsbergen (Müller et al., 2012). Continuously rising P_BIP_{25} and P_DIP_{25} in the eastern Fram Strait (Müller et al., 2012) point to extended sea-ice conditions following the Neoglacial Cooling trend (Fig. 7). This difference in sea-ice conditions between the eastern and western Fram Strait is also supported by model simulations indicating an increase of sea ice by 30% at 6 ka at the eastern Fram Strait and around Spitsbergen and only a minor increase in sea-ice concentrations at the western Fram Strait (Müller et al., 2011). The increase in sea-ice cover in the eastern Fram Strait may be explained by a declining inflow of warm Atlantic Water via the WSC (c.f., Werner et al., 2013). The western Fram Strait, on the other hand, is continuously influenced by the cold EGC and drift-ice export from the Arctic Ocean.

4.2.4. Sea-ice distribution and NEW polynya formation during the last 1 ka

During the last 1 ka, maximum concentrations and accumulation rates of IP_{25} and open-water phytoplankton and terrigenous biomarkers, as well as TOC were recorded at Core PS93/025 (Figs. 4 and 5). These significant changes are related to the seasonal formation of the NEW Polynya with suitable environmental conditions for the generation of these biomarkers. Sea ice was pushed towards the open ocean by strong katabatic winds coming from the Greenland Ice Sheet and causing the NEW Polynya to open up (Fig. 8c). Such open-water conditions in its centre and sea-ice melting at the margins caused increased fluxes of terrigenous suspension and nutrients to the surface waters within the polynya and favored primary productivity, indicated by highest brassicasterol, dinosterol and HBI III values (Fig. 4) in the NEW Polynya. The build-up of a stationary (summer) MIZ is especially reflected in the elevated HBI III concentrations (light blue field in Fig. 6b; cf., Belt et al., 2015; Ribeiro et al., 2017). Low carbonate fossil deposition (M. Zehnich, pers. comm. 2019) and low $CaCO_3$ accumulation during this interval of high productivity (Fig. 4) may result from carbonate dissolution, a process that is commonly observed in areas of high productivity and seasonal sea-ice formation (Steinsund and Hald, 1994; Knies et al., 2003). Similar findings were recorded for the recent NEW Polynya situation, where nutrients are constantly supplied by the NEGCC and favor primary productivity (Schneider and Budéus, 1997). Dissolved organic carbon occurs in a larger amount within the NEW Polynya compared to the surrounding surface waters and is most likely released by melting sea ice and ice algae (Skoog et al., 2001). Unfortunately, foraminifer assemblages from Core PS93/025 do not give a hint on carbonate dissolution during the late Holocene (Zehnich et al., 2019). Core top biomarker concentrations (uppermost 1-6 cm) in our record match very well with modern observations of sea-ice cover and TOC values in the NEW Polynya (Fig. 2a; Birgel and Stein, 2004). Knies et al. (2017) described Arctic polynyas as sea-ice factories and connected the increase in seasonal sea-ice cover with a strengthened outflow of drift ice from the Arctic Ocean along the Greenland shelves during the last 0.5 ka. Ice algae benefit from the light and nutrients availability and are able to grow within the melting sea ice (Belt et al., 2007), which would explain the elevated number of sympagic algae produced IP_{25} and HBI III (Figs. 5 and 4, interval 5). Several other studies based on foraminifer and diamicton records from East Greenland and Southeast Greenland and other marine and terrestrial proxies support a strengthening of the EGC during

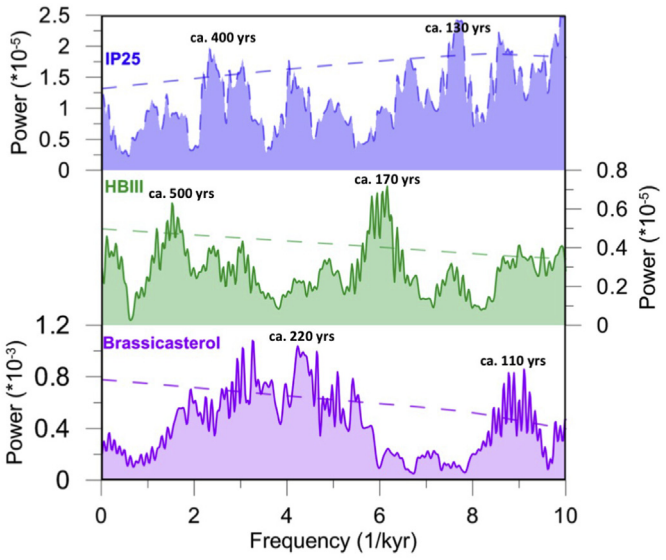

Fig. 9. LOWSPEC MTM power spectra of the Holocene (a) IP_{25} concentration, (b) HBI III concentration and (c) brassicasterol concentration at Site PS93/025. Dashed lines represent the 90% confidence level.

the last 0.6–0.7 ka (Jennings and Weiner, 1996; Nesje et al., 2000; Seppä et al., 2002; Andersson et al., 2003; Moros et al., 2006; Bendle and Rosell-Melé, 2007; Sejrup et al., 2010; Mernild et al., 2011; Cabedo-Sanz and Belt, 2016).

4.3. Short-term cyclic variability in Holocene environmental conditions

Spectral analysis reveals significant power at frequencies exceeding the 90% confidence level and corresponding to periodicities of 110–130, 170, 220 and 500 years in the proxy records of IP_{25}, HBI III and brassicasterol throughout the Holocene (Fig. 9). Such short-term cycles of 110–130 year periods have been observed in the oxygen isotope record of the NGRIP (NGRIP-Members, 2004) and are likely linked to variations in solar activity (Vonmoos et al., 2006). A spectral power centered around a period of 200 years (brassicasterol) may correspond to the De Vries/Suess cycle of solar activity. North Atlantic variability at this timescale has been previously found in the 512 year $\Delta^{14}C$ cycle and is connected to variabilities in the North Atlantic Deep Water Formation (NADW) (Stuiver and Braziunas, 1993). While the exact period of spectral peaks may be biased by uncertainties in the age model, the correspondence between our and other oceanic and terrestrial variations in paleoclimate proxies with cyclic signals in solar activity (Stuiver et al., 1995; Ito and Yu, 1999; Chapman and Shackleton, 2000; Hu et al., 2003; Zhao et al., 2010) suggests a possible key role of the amount of total solar irradiance as a driver of oceanic and atmospheric change in the Arctic region. Thus, the atmospheric response to reduced solar irradiance could lead to increasing Arctic sea-ice drift and cooling of both the ocean surface and high northern latitude continents and trigger the negative state of AO/NAO (Xu et al., 2014).

5. Conclusions

A new high-resolution biomarker record from Core PS93/025 provides new insights into the Arctic sea-ice evolution and for the first time documents the formation of the NEW Polynya on the eastern North Greenland continental shelf during the late Holocene. The presence of IP_{25} throughout the Core PS93/025 confirms that there has been seasonal sea ice in the area during the entire record. Our biomarker proxies indicate relatively rapid changes in sea-ice conditions at ~9 ka and ~1 ka, i.e., sea-ice conditions progressed through three major stages over the course of the Holocene. During the early Holocene, we recorded a reduced but variable sea-ice cover. Between about 9.3 and 5.5 ka, sea-ice coverage increased towards seasonal conditions. Based on terrigenous biomarkers and IRD we assume a stronger regional than local sea-ice signal at core site PS93/025, due to the high influence of drift ice transported from the central Arctic Ocean along the eastern North Greenland shelf. During the late Holocene, especially during the last 1 ka, our records reflect the seasonal formation of the NEW Polynya leading to stable sea-ice edge conditions and a fully developed polynya situation. Probably, cyclic changes in the solar activity acted as trigger for the short-term variability in sea-ice cover during Holocene times.

Data availability

Data related to this article are available at doi: https://doi.org/10.1594/PANGAEA.905516.

Acknowledgements

We gratefully thank Captain Wunderlich and his crew of RV *Polarstern* for the excellent support and cooperation during the entire cruise. Thanks to Walter Luttmer/AWI for technical support during the laboratory work, and Gesine Mollenhauer/AWI for high-precision express analyses of small-scale ^{14}C samples with the AWI MICADAS system. Thanks to Simon Belt (Biogeochemistry Research Centre, University of Plymouth/UK) for providing the 7-HND standard for IP_{25} quantification. Many thanks to the three anonymous reviewers for numerous constructive suggestions for improving the manuscript. ASI-AMSR2 sea ice concentration data were provided by https://seaice.uni-bremen.de/. This publication is a contribution to the Research Programme PACES II, Topic 3 (The earth system from a polar perspective: Data, modeling and synthesis) of the Alfred Wegener Institute Helmholtz Centre for Polar und Marine Research (AWI). The studied samples and data were provided by AWI (Grant No. AWI-PS93.1_01).

Appendix A. Supplementary data

Supplementary data to this article can be found online at https://doi.org/10.1016/j.quascirev.2020.106173.

References

Aagaard, K., 1982. Inflow from the Atlantic Ocean to the polar basin. In: Rey, L. (Ed.), The Arctic Ocean: the Hydrographic Environment and the Fate of Pollutants. Palgrave Macmillan UK, London, pp. 69–81. https://doi.org/10.1007/978-1-349-05919-5_3.

Aagaard, Knut, Coachman, L.K., 1968a. the East Greenland current north of Denmark strait: part I. Arctic 21, 181–200.

Aagaard, K., Coachman, L.K., 1968b. the East Greenland current north of Denmark strait: Part II. Arctic 21, 267–290.

Andersen, C., Koç, N., Jennings, A., Andrews, J.T., 2004a. Nonuniform response of the major surface currents in the Nordic Seas to insolation forcing: implications for the Holocene climate variability. Paleoceanography 19. https://doi.org/10.1029/2002PA000873.

Andersen, C., Koç, N., Moros, M., 2004b. A highly unstable Holocene climate in the subpolar North Atlantic: evidence from diatoms. Quat. Sci. Rev. 23, 2155–2166. https://doi.org/10.1016/j.quascirev.2004.08.004.

Andersson, C., Risebrobakken, B., Jansen, E., Dahl, S.O., 2003. Late Holocene surface ocean conditions of the Norwegian sea (vøring plateau). Paleoceanography 18 (2), 1044. https://doi.org/10.1029/2001PA000654.

Andrews, J.T., Darby, D., Eberle, D., Jennings, A.E., Moros, M., Ogilvie, A., 2009. A robust, multisite Holocene history of drift ice off northern Iceland: implications for North Atlantic climate. Holocene 19, 71–77. https://doi.org/10.1177/0959683608098953.

Arndt E., J., Jokat, W., Dorschel, B., 2017. The last glaciation and deglaciation of the Northeast Greenland continental shelf revealed by hydro-acoustic data. Quat. Sci. Rev. 160, 45–56. https://doi.org/10.1016/j.quascirev.2017.01.018. Submitted for publication.

Barber, D.G., Massom, R.A., 2007. Chapter 1 the role of sea ice in arctic and Antarctic polynyas. Elsevier Oceanogr. Ser. 74, 1–54. https://doi.org/10.1016/S0422-9894(06)74001-6.

Barber, D.C., Dyke, A., Hillaire-Marcel, C., Jennings, A.E., Andrews, J.T., Kerwin, M.W., Bilodeau, G., McNeely, R., Southon, J., Morehead, M.D., Gagnon, J.-M., 1999. Forcing of the cold event of 8,200 years ago by catastrophic drainage of Laurentide lakes. Nature 400, 344–348.

Bauch, H.A., Erlenkeuser, H., Spielhagen, R.F., Struck, U., Matthiessen, J., Thiede, J., Heinemeier, J., 2001. A multiproxy reconstruction of the evolution of deep and surface waters in the subarctic Nordic Seas over the last 30,000 yr. Quat. Sci. Rev. 20, 659–678. https://doi.org/10.1016/S0277-3791(00)00098-6.

Belt, S.T., 2018. Source-specific biomarkers as proxies for Arctic and Antarctic sea ice. Org. Geochem. 125, 277–298.

Belt T., S., Massé, G., Vare L., L., Rowland J., S., Poulin, M., Sicre -A., M., Sampei, M., Fortier, L., 2008. Distinctive ^{13}C isotopic signature distinguishes a novel sea ice biomarker in Arctic sediments and sediment traps. Mar. Chem. 112, 158–167. https://doi.org/10.1016/j.marchem.2008.09.002. Submitted for publication.

Belt, S.T., Müller, J., 2013. The Arctic sea ice biomarker IP_{25}: a review of current understanding, recommendations for future research and applications in palaeo sea ice reconstructions. Quat. Sci. Rev. 79, 9–25. https://doi.org/10.1016/j.quascirev.2012.12.001.

Belt, S.T., Massé, G., Rowland, S.J., Poulin, M., Michel, C., LeBlanc, B., 2007. A novel chemical fossil of palaeo sea ice: IP_{25}. Org. Geochem. 38, 16–27. https://doi.org/10.1016/j.orggeochem.2006.09.013.

Belt, S.T., Cabedo-Sanz, P., Smik, L., Navarro-Rodriguez, A., Berben, S.M.P., Knies, J., Husum, K., 2015. Identification of paleo Arctic winter sea ice limits and the marginal ice zone: optimised biomarker-based reconstructions of late Quaternary Arctic sea ice. Earth Planet. Sci. Lett. 431, 127–139. https://doi.org/10.1016/j.epsl.2015.09.020.

Belt, S.T., Smik, L., Köseo, D., Knies, J., Husum, K., 2019. A novel biomarker-based proxy for the spring phytoplankton bloom in Arctic and sub-arctic settings – HBI T_{25}. Earth Planet. Sci. Lett. 523, 115703 https://doi.org/10.1016/j.epsl.2019.06.038.

Bendle, J.A.P., Rosell-Melé, A., 2007. High-resolution alkenone sea surface temperature variability on the North Icelandic Shelf: implications for Nordic Seas palaeoclimatic development during the holocene. Holocene 17, 9–24. https://doi.org/10.1177/0959683607073269.

Bennike, O., 2004. Holocene sea-ice variations in Greenland: onshore evidence. Holocene 14, 607–613. https://doi.org/10.1191/0959683604hl722rr.

Bennike, O., Weidick, A., 2001. Late quaternary history around nioghalvfjerdsfjorden and jøkelbugten, north-east Greenland. Boreas 30, 205–227. https://doi.org/10.1111/j.1502-3885.2001.tb01223.x.

Berben, S.M.P., Husum, K., Navarro-Rodriguez, A., Belt, S.T., Aagaard-Sørensen, S., 2017. Semi-quantitative reconstruction of early to late Holocene spring and summer sea ice conditions in the northern Barents sea. J. Quat. Sci. 32, 587–603. https://doi.org/10.1002/jqs.2953.

Birgel, D., Stein, R., 2004. Northern Fram Strait und Yermak Plateau: distribution, Variability and Burial of Organic Carbon and Paleoenvironmental implications. In: Stein, R., Macdonald, R.W. (Eds.), The Organic Carbon Cycle in the Arctic Ocean. Springer-Verlag, Berlin, pp. 279–294.

Blaschek, M., Renssen, H., 2013. The impact of early Holocene Arctic shelf flooding on climate in an atmosphere–ocean–sea–ice model. Clim. Past 9, 2651–2667. https://doi.org/10.5194/cp-9-2651-2013.

Boon, J.J., Rijpstra, W.I.C., De Lange, F., De Leeuw, J.W., Yoshioka, M., Shimizu, Y., 1979. Black Sea sterol - a molecular fossil for dinoflagellate blooms. Nature 277, 125–127. https://doi.org/10.1038/277125a0.

Bourke, R.H., Garrett, R.P., 1987. Sea ice thickness distribution in the Arctic ocean. Cold Reg. Sci. Technol. 13, 259–280. https://doi.org/10.1016/0165-232X(87)90007-3.

Briner, J.P., McKay, N.P., Axford, A., Bennike, O., Bradley, R.S., de Vernal, A., Fisher, D., Francus, P., Fréchette, B., Gajewski, K., Jennings, A., Kaufman, D.S., Miller, G., Rouston, C., Wagner, B., 2016. Holocene climate change in Arctic Canada and Greenland. Quat. Sci. Rev. 147, 340–364.

Brown, T.A., Belt, S.T., 2016. Novel tri- and tetra-unsaturated highly branched isoprenoid (HBI) alkenes from the marine diatom Pleurosigma intermedium. Org. Geochem. 91, 120–122. https://doi.org/10.1016/j.orggeochem.2015.11.008.

Brown, T.A., Belt, S.T., Tatarek, A., Mundy, C.J., 2014. Source identification of the Arctic sea ice proxy IP_{25}. Nat. Commun. 5, 1–7. https://doi.org/10.1038/ncomms5197.

Budéus, G., Schneider, W., 1995. On the hydrography of the Northeast water polynya. J. Geophys. Res. Ocean. 100, 4287–4299. https://doi.org/10.1029/94JC02024.

Cabedo-Sanz, P., Belt, S.T., 2016. Seasonal sea ice variability in eastern Fram Strait over the last 2000 years. Arktos 2, 22. https://doi.org/10.1007/s41063-016-0023-2.

Cabedo-Sanz, P., Belt, S.T., Jennings, A.E., Andrews, J.T., Geirsdóttir, Á., 2016. Variability in drift ice export from the Arctic Ocean to the North Icelandic Shelf over the last 8000 years: a multi-proxy evaluation. Quat. Sci. Rev. 146, 99–115. https://doi.org/10.1016/j.quascirev.2016.06.012.

Carstens, J., Hebbeln, D., Wefer, G., 1997. Distribution of planktic foraminifera at the ice margin in the Arctic (Fram strait). Mar. Micropaleontol. 29, 257–269.

Chapman, M.R., Shackleton, N.J., 2000. Evidence of 550-year and 1000-year cyclicities in north Atlantic circulation patterns during the holocene. Holocene 10, 287–291. https://doi.org/10.1191/095968300671253196.

Cleveland, W.S., 1979. Robust locally weighted regression and smoothing scatterplots. J. Am. Stat. Assoc. 74, 829–836. https://doi.org/10.1080/01621459.1979.10481038.

Collins, L.G., Allen, C.S., Pike, J., Hodgson, D.A., Weckström, K., Massé, G., 2013. Evaluating highly branched isoprenoid (HBI) biomarkers as a novel Antarctic sea-ice proxy in deep ocean glacial age sediments. Quat. Sci. Rev. 79, 87–98. https://doi.org/10.1016/j.quascirev.2013.02.004.

Darby, D., Ortiz, J., Grosch, C., et al., 2012. 1,500-year cycle in the Arctic Oscillation identified in Holocene Arctic sea-ice drift. Nat. Geosci. 5, 897–900. https://doi.org/10.1038/ngeo1629.

de Vernal, A., Gersonde, R., Goosse, H., Seidenkrantz, M.-S., Wolff, E.W., 2013. Sea ice in the paleoclimate system: the challenge of reconstructing sea ice from proxies – an introduction. Quat. Sci. Rev. 79, 1–8. https://doi.org/10.1016/j.quascirev.2013.08.009.

Dieckmann, G.S., Hellmer, H.H., 2003. The importance of sea ice: an overview. In: Thomas, D.N., Dieckmann, G.S. (Eds.), Sea Ice: an Introduction to its Physics, Chemistry, Biology and Geology. Blackwell Science Ltd, Oxford, UK. https://doi.org/10.1002/9780470757161.ch1.

Eicken, H., Lensu, M., Leppäranta, M., Tucker III, W.B., Gow, A.J., Salmela, O., 1995. Thickness, structure, and properties of level summer multiyear ice in the Eurasian sector of the Arctic Ocean. J. Geophys. Res. Ocean. 100, 22697–22710. https://doi.org/10.1029/95JC02188.

Fahl, K., Stein, R., 1999. Biomarkers as organic-carbon-source and environmental indicators in the Late Quaternary Arctic Ocean: problems and perspectives. Mar. Chem. 63, 293–309. https://doi.org/10.1016/S0304-4203(98)00068-1.

Fahl, K., Stein, R., 2012. Modern seasonal variability and deglacial/Holocene change of central Arctic Ocean sea-ice cover: new insights from biomarker proxy records. Earth Planet. Sci. Lett. 351–352, 123–133. https://doi.org/10.1016/j.epsl.2012.07.009.

Funder, S., Goosse, H., Jepsen, H., Kaas, E., Kjær, K.H., Korsgaard, N.J., Larsen, N.K., Linderson, H., Lysså, A., Möller, P., Olsen, J., Willerslev, E., 2011. A 10,000-year record of Arctic Ocean sea-ice variability – view from the beach. Science 333, 747–750. https://doi.org/10.1126/science.1202760.

Grootes, P.M., Stuiver, M., White, J.W.C., Johnsen, S., Jouzel, J., 1993. Comparison of oxygen isotope records from the GISP2 and GRIP Greenland ice cores. Nature 366, 552–554. https://doi.org/10.1038/366552a0.

Hirche, H.-J., Baumann, M.E.M., Kattner, G., Gradinger, R., 1991. Plankton distribution and the impact of copepod grazing on primary production in Fram Strait, Greenland sea. J. Mar. Syst. 2, 477–494. https://doi.org/10.1016/0924-7963(91)90048-Y.

Hjort, C., Funder, S., 1974. The subfossil occurrence of Mytilus edulis L. in central East Greenland. Boreas 3, 23–33. https://doi.org/10.1111/j.1502-3885.1974.tb00664.x.

Hörner, T., Stein, R., Fahl, K., Birgel, D., 2016. Post-glacial variability of sea ice cover, river run-off and biological production in the western Laptev Sea (Arctic Ocean) – a high-resolution biomarker study. Quat. Sci. Rev. 143, 133–149. https://doi.org/10.1016/j.quascirev.2016.04.011.

Hu, F.S., Kaufman, D., Yoneji, S., Nelson, D., Shemesh, A., Huang, Y., Tian, J., Bond, G., Clegg, B., Brown, T., 2003. Cyclic variation and solar forcing of Holocene climate in the Alaskan subarctic. Science 301, 1890–1893. https://doi.org/10.1126/science.1088568.

Ito, E., Yu, Z., 1999. Possible solar forcing of century-scale drought frequency in the northern Great plains. Geology 27, 263–266. https://doi.org/10.1130/0091-7613(1999)027<0263:PSFOCS>2.3.CO;2.

James, N.A., Matteson, D.S., 2013. Ecp: an R package for nonparametric multiple change point Analysis of multivariate data. J. Stat. Softw. 62, 1–25. https://doi.org/10.18637/jss.v062.i07.

Jennings, A.E., Weiner, N.J., 1996. Environmental change in eastern Greenland during the last 1300 years: evidence from foraminifera and lithofacies in Nansen Fjord, 68°N. Holocene 6, 179–191. https://doi.org/10.1177/095968369600600205.

Jennings, A.E., Knudsen, K.L., Hald, M., Hansen, V., Andrews, J.T., Hansen, C.V., Andrews, J.T., Hansen, V., Andrews, J.T., Hansen, C.V., Andrews, J.T., 2002. A mid-Holocene shift in Arctic sea-ice variability on the East Greenland shelf. Holocene 12, 49–58. https://doi.org/10.1191/0959683602hl519rp.

Joughin, I., Smith, B.E., Howat, I.M., Scambos, T., Moon, T., 2010. Greenland flow variability from ice-sheet-wide velocity mapping. J. Glaciol. 56, 415–430. https://doi.org/10.3189/002214310792447734.

Kaufman, D.S., Ager, T.A., Anderson, N.J., Anderson, P.M., Andrews, J.T., Bartlein, P.J., Brubaker, L.B., Coats, L.L., Cwynar, L.C., Duvall, M.L., Dyke, A.S., Edwards, M.E., Eisner, W.R., Gajewski, K., Geirsdóttir, A., Hu, F.S., Jennings, A.E., Kaplan, M.R., Kerwin, M.W., Lozhkin, A.V., MacDonald, G.M., Miller, G.H., Mock, C.J., Oswald, W.W., Otto-Bliesner, B.L., Porinchu, D.F., Rühland, K., Smol, J.P., Steig, E.J., Wolfe, B.B., 2004. Holocene thermal maximum in the western Arctic (0–180°W). Quat. Sci. Rev. 23, 529–560. https://doi.org/10.1016/j.quascirev.2003.09.007.

Knies, J., Hald, M., Ebbesen, H., Mann, U., Vogt, C., 2003. A deglacial – middle Holocene record of biogenic sedimentation and paleoproductivity changes from the northern Norwegian continental shelf. Paleoceanography 18, 1096. https://doi.org/10.1029/2002PA000872.

Knies, J., Pathirana, I., Cabedo-Sanz, P., Banica, A., Fabian, K., Rasmussen, T.L., Forwick, M., Belt, S.T., 2017. Sea-ice dynamics in an Arctic coastal polynya during the past 6500 years. Arktos 3, 1. https://doi.org/10.1007/s41063-016-0027-y.

Kobashi, T., Severinghaus, J.P., Brook, E.J., Barnola, J.M., Grachev, A.M., 2007. Precise timing and characterization of abrupt climate change 8200 years ago from air trapped in polar ice. Quat. Sci. Rev. 26, 1212–1222.

Koç, N., Jansen, E., Haflidason, H., 1993. Paleoceanographic reconstructions of surface ocean conditions in the Greenland, Iceland and Norwegian Seas through the last 14 ka based on diatoms. Quat. Sci. Rev. 12, 115–140. https://doi.org/10.1016/0277-, 3791(93)90012-B.

Kuklinski, P., Bader, B., 2007. Diversity, structure and interactions of encrusting lithophyllic macrofaunal assemblages from Belgica Bank, East Greenland. Polar Biol. 30, 709–717. https://doi.org/10.1007/s00300-006-0228-0.

Laskar, J., Robutel, P., Joutel, F., Gastineau, M., Correia, A.C.M., Levrard, B., 2004. A long-term numerical solution for the insolation quantities of the Earth. A&A 428, 261–285. https://doi.org/10.1051/0004-6361:20041335.

Lecavalier, B.S., Fisher, D.A., Milne, G.A., Vinther, B.M., Tarasov, L., Huybrechts, P., Lacelle, D., Main, B., Zheng, J., Bourgeois, J., Dyke, A.S., 2017. High Arctic Holocene temperature record from the Agassiz ice cap and Greenland ice sheet evolution. Proc. Natl. Acad. Sci. 114, 5952–5957. https://doi.org/10.1073/pnas.1616287114.

Limoges, A., Ribeiro, S., Weckström, K., Heikkilä, M., Zamelczyk, K., Andersen, T.J., Tallberg, P., Massé, G., Rysgaard, S., Nørgaard-Pedersen, N., Seidenkrantz, M.-S., 2018. Linking the modern distribution of biogenic proxies in high arctic Greenland shelf sediments to sea ice, primary production, and arctic-Atlantic inflow. J. Geophys. Res. Biogeosciences 123, 760–786. https://doi.org/10.1002/2017JG003840.

Ljungqvist, F.C., 2010. A new reconstruction of temperature variability in the extra tropical northern Hemisphere during the last two millennia. Geogr. Ann. Ser. A Phys. Geogr. 92, 339–351. https://doi.org/10.1111/j.1468-0459.2010.00399.x.

Loeb, V., Siegel, V., Holm-Hansen, O., Hewitt, R., Fraser, W., Trivelpiece, W., Trivelpiece, S., 1997. Effects of sea-ice extent and krill or salp dominance on the Antarctic food web. Nature 387, 897.

Manabe, S., Spelman, M.J., Stouffer, R.J., 1992. Transient responses of a coupled

ocean-atmosphere model to gradual changes of atmospheric CO_2. Part II: seasonal response. J. Clim. 5, 105–126. https://doi.org/10.1175/1520-0442(1992)005<0105:TROACO>2.0.CO;2.
Mayewski, P.A., Rohling, E.E., Curt Stager, J., Karlén, W., Maasch, K.A., Meeker, L.D., Meyerson, E.A., Gasse, F., van Kreveld, S., Holmgren, K., Lee-Thorp, J., Rosqvist, G., Rack, F., Staubwasser, M., Schneider, R.R., Steig, E.J., 2004. Holocene climate variability. Quat. Res. 62, 243–255. https://doi.org/10.1016/j.yqres.2004.07.001.
Mernild, S.H., Seidenkrantz, M.-S., Chylek, P., Liston, G.E., Hasholt, B., 2011. Climate-driven fluctuations in freshwater flux to Sermilik Fjord, East Greenland, during the last 4000 years. Holocene 22, 155–164. https://doi.org/10.1177/0959683611431215.
Meyers, S.R., 2012. Seeing red in cyclic stratigraphy: spectral noise estimation for astrochronology. Paleoceanography 27, 1–12. https://doi.org/10.1029/2012PA002307.
Moros, M., Andrews, J.T., Eberl, D.D., Jansen, E., 2006. Holocene history of drift ice in the northern North Atlantic: evidence for different spatial and temporal modes. Paleoceanography 21. https://doi.org/10.1029/2005PA001214.
Müller, J., Massé, G., Stein, R., Belt, S.T., 2009. Variability of sea-ice conditions in the Fram Strait over the past 30,000 years. Nat. Geosci. 2, 772.
Müller, J., Wagner, A., Fahl, K., Stein, R., Prange, M., Lohmann, G., 2011. Towards quantitative sea ice reconstructions in the northern North Atlantic: a combined biomarker and numerical modelling approach. Earth Planet. Sci. Lett. 306, 137–148. https://doi.org/10.1016/j.epsl.2011.04.011.
Müller, J., Werner, K., Stein, R., Fahl, K., Moros, M., Jansen, E., 2012. Holocene cooling culminates in sea ice oscillations in Fram strait. Quat. Sci. Rev. 47, 1–14. https://doi.org/10.1016/j.quascirev.2012.04.024.
http://nsidc.org/, 2017.
Nesje, A., Olaf Dahl, S., Andersson, C., Matthews, J.A., 2000. The lacustrine sedimentary sequence in Sygneskardvatnet, western Norway: a continuous, high-resolution record of the Jostedalsbreen ice cap during the holocene. Quat. Sci. Rev. 19, 1047–1065. https://doi.org/10.1016/S0277-3791(99)00090-6.
Ngrip-Members, 2004. High-resolution record of Northern Hemisphere climate extending into the last interglacial period. Nature 431, 147–151.
Notz, D., Stroeve, J., 2018. The trajectory towards a seasonally ice-free Arctic ocean. Curr. Clim. Chang. Rep. 4, 407–416. https://doi.org/10.1007/s40641-018-0113-2.
Overland, J.E., Wang, M., 2005. The Arctic climate paradox: the recent decrease of the Arctic oscillation. Geophys. Res. Lett. 32 https://doi.org/10.1029/2004GL021752.
Pados, T., Spielhagen, R.F., 2014. Species distribution and depth habitat of recent planktic foraminifera in Fram Strait, Arctic Ocean. Polar Res. 33, 22483. https://doi.org/10.3402/polar.v33.22483.
Parnell, A.C., Haslett, J., Allen, J.R.M., Buck, C.E., Huntley, B., 2008. A flexible approach to assessing synchroneity of past events using Bayesian reconstructions of sedimentation history. Quat. Sci. Rev. 27, 1872–1885. https://doi.org/10.1016/j.quascirev.2008.07.009.
Pieńkowski, A.J., Gill, N.K., Furze, M.F.A., Mugo, S.M., Marret, F., Perreaux, A., 2016. Arctic sea-ice proxies: comparisons between biogeochemical and micro-palaeontological reconstructions in a sediment archive from Arctic Canada. Holocene 27, 665–682. https://doi.org/10.1177/0959683616670466.
Ran, L., Jiang, H., Knudsen, K.L., Eiríksson, J., Gu, Z., 2006. Diatom response to the Holocene climatic optimum on the North Icelandic shelf. Mar. Micropaleontol. 60, 226–241. https://doi.org/10.1016/j.marmicro.2006.05.002.
Randall, D., Curry, J., Battisti, D., Flato, G., Grumbine, R., Hakkinen, S., Martinson, D., Preller, R., Walsh, J., Weatherly, J., 1998. Status of and outlook for large-scale modeling of atmosphere–ice–ocean interactions in the arctic. Bull. Am. Meteorol. Soc. 79, 197–220. https://doi.org/10.1175/1520-0477(1998)079<0197:SOAOFL>2.0.CO;2.
Rasmussen, S.O., Vinther, B.O., Clausen, H.B., Andersen, K.K., 2007. Early Holocene climate oscillations recorded in three Greenland ice cores. Quat. Sci. Rev. 26, 1907–1914.
Reeh, N., 2004. Holocene climate and fjord glaciations in Northeast Greenland: implications for IRD deposition in the North Atlantic. Sediment. Geol. 165, 333–342. https://doi.org/10.1016/j.sedgeo.2003.11.023.
Reimer, P.J., Bard, E., Bayliss, A., Beck, J.W., Blackwell, P.G., Ramsey, C.B., Buck, C.E., Cheng, H., Edwards, R.L., Friedrich, M., Grootes, P.M., Guilderson, T.P., Haflidason, H., Hajdas, I., Hatté, C., Heaton, T.J., Hoffmann, D.L., Hogg, A.G., Hughen, K.A., Kaiser, K.F., Kromer, B., Manning, S.W., Niu, M., Reimer, R.W., Richards, D.A., Scott, E.M., Southon, J.R., Staff, R.A., Turney, C.S.M., van der Plicht, J., 2013. IntCal13 and Marine13 radiocarbon age calibration curves 0–50,000 Years cal BP. Radiocarbon 55, 1869–1887. https://doi.org/10.2458/azu_js_rc.55.16947.
Reimnitz, E., Kassens, H., Eicken, H., 1995. Sediment transport by laptav sea ice. Rep. Polar Res. 176, 71–77.
Renssen, H., Goosse, H., Muscheler, R., 2006. Coupled climate model simulation of Holocene cooling events: solar forcing triggers oceanic feedback. Clim. Past Discuss. 2, 209–232. https://doi.org/10.5194/cpd-2-209-2006.
Ribeiro, S., Sejr, M.K., Limoges, A., Heikkilä, M., Andersen, T.J., Tallberg, P., Weckström, K., Husum, K., Forwick, M., Dalsgaard, T., Massé, G., Seidenkrantz, M.-S., Rysgaard, S., 2017. Sea ice and primary production proxies in surface sediments from a High Arctic Greenland fjord: spatial distribution and implications for palaeoenvironmental studies. Ambio 46, 106–118. https://doi.org/10.1007/s13280-016-0894-2.
Rignot, E., Kanagaratnam, P., 2006. Changes in the velocity structure of the Greenland ice sheet. Science 311, 986–990. https://doi.org/10.1126/science.1121381.
Rignot, E., Velicogna, I., van den Broeke, M.R., Monaghan, A., Lenaerts, J.T.M., 2011. Acceleration of the contribution of the Greenland and Antarctic ice sheets to sea level rise. Geophys. Res. Lett. 38, L05503. https://doi.org/10.1029/2011GL046583.
Rohling, E.J., Pälike, H., 2005. Centennial-scale climate cooling with a sudden cold event around 8,200 years ago. Nature 434, 975.
Ruckstuhl, A.F., Jacobson, M.P., Field, R.W., Dodd, J.A., 2001. Baseline subtraction using robust local regression estimation. J. Quant. Spectrosc. Radiat. Transf. 68, 179–193. https://doi.org/10.1016/S0022-4073(00)00021-2.
Rudels, B., Quadfasel, D., 1991. Convection and deep Water Formation in the Arctic Ocean-Greenland sea system. J. Mar. Syst. 2, 435–450. https://doi.org/10.1016/0924-7963(91)90045-V.
Rudels, B., Anderson, L.G., Jones, E.P., 1996. Formation and evolution of the surface mixed layer and halocline of the Arctic ocean. J. Geophys. Res. Ocean 101, 8807–8821. https://doi.org/10.1029/96JC00143.
Rudels, B., Friedrich, J., H, Quadfasel, D., 1999. The arctic circumpolar boundary current. Deep Sea Res. Part II Top. Stud. Oceanogr. 46, 1023–1062. https://doi.org/10.1016/S0967-0645(99)00015-6.
Rigor, I.G., Wallace, J.M., Colony, R.L., 2002. Response of sea ice to the arctic oscillation. J. Clim. 15, 2648–2663. https://doi.org/10.1175/1520-0442(2002)015<2648:ROSITT>2.0.CO;2.
Schlichtholz, P., Houssais, M.-N., 1999. An inverse modeling study in Fram Strait. Part I: dynamics and circulation. Deep Sea Res. Part II Top. Stud. Oceanogr. 46, 1083–1135. https://doi.org/10.1016/S0967-0645(99)00018-1.
Schneider, W., Budéus, G., 1994. The north East water polynya (Greenland sea). Polar Biol. 14, 1–9. https://doi.org/10.1007/BF00240265.
Schneider, W., Budéus, G., 1997. Summary of the Northeast water polynya formation and development (Greenland sea). J. Mar. Syst. 10, 107–122. https://doi.org/10.1016/S0924-7963(96)00075-9.
Screen, J.A., Simmonds, I., 2010. The central role of diminishing sea ice in recent Arctic temperature amplification. Nature 464, 1334.
Sejrup, H.P., Lehman, S.J., Haflidason, H., Noone, D., Muscheler, R., Berstad, I.M., Andrews, J.T., 2010. Response of Norwegian Sea temperature to solar forcing since 1000 A. D. J. Geophys. Res. 115, 1–10. https://doi.org/10.1029/2010JC006264.
Seppä, H., Birks, H.H., Birks, H.J.B., 2002. Rapid climatic changes during the Greenland stadial 1 (Younger Dryas) to early Holocene transition on the Norwegian Barents Sea coast. Boreas 31, 215–225. https://doi.org/10.1111/j.1502-3885.2002.tb01068.x.
Serreze, M.C., Stroeve, J., Barrett, A.P., Boisvert, L.N., 2016. J. Geophys. Res.: Atmosphere 2, 463–485. https://doi.org/10.1002/2016JD025161.
Sévellec, F., Fedorov, A.V., Liu, W., 2017. Arctic sea-ice decline weakens the Atlantic meridional overturning circulation. Nat. Clim. Chang. 7, 604.
Skoog, A., Lara, R., Kattner, G., 2001. Spring–summer cycling of DOC, DON and inorganic N in a highly seasonal system encompassing the Northeast Water Polynya, 1993. Deep-Sea Res. Part I Oceanogr. Res. Pap. 48, 2613–2629. https://doi.org/10.1016/S0967-0637(01)00029-2.
Smedsrud, L.H., Halvorsen, M.H., Stroeve, J.C., Zhang, R., Kloster, K., 2017. Fram Strait sea ice export variability and September Arctic sea ice extent over the last 80 years. Cryosphere 11, 65–79. https://doi.org/10.5194/tc-11-65-2017.
Smik, L., Cabedo-Sanz, P., Belt, S.T., 2016. Semi-quantitative estimates of paleo Arctic sea ice concentration based on source-specific highly branched isoprenoid alkenes: a further development of the PIP_{25} index. Org. Geochem. 92, 63–69. https://doi.org/10.1016/j.orggeochem.2015.12.007.
Smith, S.D., Muench, R.D., Pease, C.H., 1990. Polynyas and leads: an overview of physical processes and environment. J. Geophys. Res. Ocean. 95, 9461–9479. https://doi.org/10.1029/JC095iC06p09461.
Spreen, G., Kaleschke, L., Heygster, G., 2008. Sea ice remote sensing using AMSR-E 89 GHz channels. J. Geophys. Res. 113, C02S03. https://doi.org/10.1029/2005JC003384.
Stein, R., 2016. The Expedition PS93.1 of the Research Vessel POLARSTERN to the Greenland Sea and the Fram Strait in 2015. Berichte zur Polar- und Meeresforschung. Reports on polar and marine research, Bremerhaven. Alfred Wegener Institute for Polar and Marine Research 695, 151. https://doi.org/10.2312/BzPM_0695_2016.
Stein, R., Macdonald, R.W., 2004. Geochemical proxies used for organic carbon source identification in Arctic Ocean sediments. In: Stein, R., Macdonald, R.W. (Eds.), The Organic Carbon Cycle in the Arctic Ocean. Springer-Verlag, Berlin, pp. 24–30.
Stein, R., Fahl, K., Müller, J., 2012. Proxy reconstruction of cenozoic Arctic Ocean sea-ice history – from IRD to IP_{25}. Polarforschung 82, 37–71.
Stein, R., Fahl, K., Schade, I., Manerung, A., Wassmuth, S., Niessen, F., Nam, S. Il, 2017. Holocene variability in sea ice cover, primary production, and Pacific-Water inflow and climate change in the Chukchi and East Siberian seas (Arctic Ocean). J. Quat. Sci. 32, 362–379. https://doi.org/10.1002/jqs.2929.
Steinsund, P.I., Hald, M., 1994. Recent calcium carbonate dissolution in the Barents Sea: paleoceanographic applications. Mar. Geol. 117, 303–316. https://doi.org/10.1016/0025-3227(94)90022-1.
Stirling, I., 1980. The biological importance of polynyas in the Canadian arctic. Arctic 33, 303–315.
Stroeve, J.C., Serreze, M.C., Holland, M.M., Kay, J.E., Malanik, J., Barrett, A.P., 2012. The Arctic's rapidly shrinking sea ice cover: a research synthesis. Clim. Change 110, 1005–1027. https://doi.org/10.1007/s10584-011-0101-1.
Stuiver, M., Braziunas, T.F., 1993. Sun, Ocean, climate and atmospheric $^{14}CO_2$: an

evaluation of causal and spectral relationships. Holocene 3, 289–305. https://doi.org/10.1177/095968369300300401.
Stuiver, M., Grootes, P.M., Braziunas, T.F., 1995. The GISP2 $\delta^{18}O$ climate record of the past 16,500 Years and the role of the sun, ocean, and volcanoes. Quat. Res. 44, 341–354. https://doi.org/10.1006/qres.1995.1079.
Stuiver, M., Reimer, P.J., Reimer, R.W., 2019. CALIB 7.1 [WWW program] at. accessed 2019-8-14. http://calib.org.
Sundqvist, H.S., Kaufman, D.S., McKay, N.P., Balascio, N.L., Briner, J.P., Cwynar, L.C., Sejrup, H.P., Seppä, H., Subetto, D.A., Andrews, J.T., Axford, Y., Bakke, J., Birks, H.J.B., Brooks, S.J., De Vernal, A., Jennings, A.E., Ljungqvist, F.C., Rühland, K.M., Saenger, C., Smol, J.P., Viau, A.E., 2014. Arctic Holocene proxy climate database – new approaches to assessing geochronological accuracy and encoding climate variables. Clim. Past 10, 1605–1631. https://doi.org/10.5194/cp-10-1605-2014.
Telesiński, M.M., Spielhagen, R.F., Bauch, H.A., 2014. Water mass evolution of the Greenland Sea since late glacial times. Clim. Past 10, 123–136. https://doi.org/10.5194/cp-10-123-2014.
Thomas, D.N., Dieckmann, G.S., 2008. sea ice: an introduction to its physics. Chem. Biol. Geol. 1–22.
Thomas, E.R., Wolff, E.W., Mulvaney, R., Steffensen, J.P., Johnsen, S.J., Arrowsmith, C., White, J.W.C., Vaughn, B., Popp, T., 2007. The 8.2 ka event from Greenland ice cores. Quat. Sci. Rev. 26, 70–81.
Thomson, D.J., 1982. Spectrum estimation and harmonic analysis. Proc. IEEE 70, 1055–1096. https://doi.org/10.1109/PROC.1982.12433.
Vinje, T., 1977. Sea ice conditions in the European sector of the marginal seas of the Arctic, 1966e1975. Nor. Polarinst. Arbok 1975, 163–174.
Volkman, J.K., 1986. A review of sterol markers for marine and terrigenous organic matter. Org. Geochem. 9, 83–99. https://doi.org/10.1016/0146-6380(86)90089-6.
Volkmann, R., 2000. Planktic foraminifer ecology and stable isotope geochemistry in the Arctic Ocean: implications from water column and sediment surface studies for quantitative reconstructions of oceanic parameters. Ber. Polarforsch. 361, 61–86.
Vonmoos, M., Beer, J., Muscheler, R., 2006. Large variations in Holocene solar activity: constraints from ^{10}Be in the Greenland ice core project ice core. J. Geophys. Res. Sp. Phys. 111, 1–14. https://doi.org/10.1029/2005JA011500.
Wadhams, P., 1981. The ice cover in the Greenland and Norwegian seas. Rev. Geophys. 19, 345–393. https://doi.org/10.1029/RG019i003p00345.
Walsh, J.E., Fetterer, F., Scott Stewart, J., Chapman, W.L., 2017. A database for depicting Arctic sea ice variations back to 1850. Geogr. Rev. 107, 89–107. https://doi.org/10.1111/j.1931-0846.2016.12195.x.
Waniek, J.J., Holliday, N.P., Davidson, R., Brown, L., Henson, S.A., 2005. Freshwater control of onset and species composition of Greenland shelf spring bloom. MEPS 288, 45–57.
Wanner, H., Solomina, O., Grosjean, M., Ritz, S.P., Jetel, M., 2011. Structure and origin of Holocene cold events. Quat. Sci. Rev. 30, 3109–3123. https://doi.org/10.1016/j.quascirev.2011.07.010.
Werner, K., Spielhagen, R.F., Bauch, D., Hass, H.C., Kandiano, E., 2013. Atlantic Water advection versus sea-ice advances in the eastern Fram Strait during the last 9 ka: multiproxy evidence for a two-phase holocene. Paleoceanography 28, 283–295. https://doi.org/10.1002/palo.20028.
World Meteorological Organization, 1970. WMO sea ice nomenclature. WMO Rep 259. https://worldview.earthdata.nasa.gov/. TP 1.
World Meteorological Organization, 1985. WMO sea ice nomenclature. WMO Rep 259. TP 145.
Xiao, X., Fahl, K., Stein, R., 2013. Biomarker distributions in surface sediments from the Kara and Laptev seas (Arctic Ocean): indicators for organic-carbon sources and sea-ice coverage. Quat. Sci. Rev. 79, 40–52. https://doi.org/10.1016/j.quascirev.2012.11.028.
Xiao, X., Fahl, K., Müller, J., Stein, R., 2015. Sea-ice distribution in the modern Arctic Ocean: biomarker records from trans-Arctic Ocean surface sediments. Geochem. Cosmochim. Acta 155, 16–29. https://doi.org/10.1016/j.gca.2015.01.029.
Xu, D., Lu, H., Chu, G., Wu, N., Shen, C., Wang, C., Mao, L., 2014. 500-year climate cycles stacking of recent centennial warming documented in an East Asian pollen record. Sci. Rep. 4, 3611. https://doi.org/10.1038/srep03611.
Yu, S.H., Colman, S.M., Lowell, T.V., Milne, G.A., Fisher, T.G., Breckenridge, A., Boyd, M., Teller, J.T., 2010. Freshwater outburst from Lake Superior as a trigger for the cold event 9300 years ago. Science 328, 1262–1266.
Zehnich, M., Spielhagen, R., Bauch, H.A., Forwick, M., Hass, H.C., Mollenhauer, G., Palme, T., Stein, R., Syring, N., 2019. Environmental variability off NE Greenland (western Fram Strait) during the holocene. Geophys. Res. Abstr. 21. EGU2019-15402.
Zhao, C., Yu, Z., Ito, E., Zhao, Y., 2010. Holocene climate trend, variability, and shift documented by lacustrine stable-isotope record in the northeastern United States. Quat. Sci. Rev. 29, 1831–1843. https://doi.org/10.1016/j.quascirev.2010.03.018.